agronomy

MDPI

Article

Analysis of Carbon Emissions and Ecosystem Service Value Caused by Land Use Change, and Its Coupling Characteristics in the Wensu Oasis, Northwest China

Yiqi Zhao [1], Songrui Ning [1,*], An Yan [2], Pingan Jiang [3], Huipeng Ren [1], Ning Li [1], Tingting Huo [1] and Jiandong Sheng [3]

[1] State Key Laboratory of Water Engineering Ecology and Environment in Arid Area, Xi'an University of Technology, Xi'an 710048, China; 18103416163@163.com (Y.Z.); 15664663950@163.com (H.R.); 17590693657@163.com (N.L.); 19803141320@163.com (T.H.)
[2] College of Grassland Science, Xinjiang Agricultural University, Urumqi 830052, China; zryanan@163.com
[3] College of Resources and Environment, Xinjiang Agricultural University, Urumqi 830052, China; jpa@xjau.edu.cn (P.J.); sjd@xjau.edu.cn (J.S.)
* Correspondence: ningsongrui@163.com

Abstract

Oases in arid regions are crucial for sustaining agricultural production and ecological stability, yet few studies have simultaneously examined the coupled dynamics of land use/cover change (LUCC), carbon emissions, and ecosystem service value (ESV) at the oasis–agricultural scale. This gap limits our understanding of how different land use trajectories shape trade-offs between carbon processes and ecosystem services in fragile arid ecosystems. This study examines the spatiotemporal interactions between land use carbon emissions and ESV from 1990 to 2020 in the Wensu Oasis, Northwest China, and predicts their future trajectories under four development scenarios. Multi-period remote sensing data, combined with the carbon emission coefficient method, modified equivalent factor method, spatial autocorrelation analysis, the coupling coordination degree model, and the PLUS model, were employed to quantify LUCC patterns, carbon emission intensity, ESV, and its coupling relationships. The results indicated that (1) cultivated land, construction land, and unused land expanded continuously (by 974.56, 66.77, and 1899.36 km^2), while grassland, forests, and water bodies declined (by 1363.93, 77.92, and 1498.83 km^2), with the most pronounced changes occurring between 2000 and 2010; (2) carbon emission intensity increased steadily—from 23.90 $\times$ 10^4 t in 1990 to 169.17 $\times$ 10^4 t in 2020—primarily driven by construction land expansion—whereas total ESV declined by 46.37%, with water and grassland losses contributing substantially; (3) carbon emission intensity and ESV exhibited a significant negative spatial correlation, and the coupling coordination degree remained low, following a "high in the north, low in the south" distribution; and (4) scenario simulations for 2030–2050 suggested that this negative correlation and low coordination will persist, with only the ecological protection scenario (EPS) showing potential to enhance both carbon sequestration and ESV. Based on spatial clustering patterns and scenario outcomes, we recommend spatially differentiated land use regulation and prioritizing EPS measures, including glacier and wetland conservation, adoption of water-saving irrigation technologies, development of agroforestry systems, and renewable energy utilization on unused land. By explicitly linking LUCC-driven carbon–ESV interactions with scenario-based prediction and evaluation, this study provides new insights into oasis sustainability, offers a scientific basis for balancing agricultural production with ecological protection in the oasis of the arid region, and informs China's dual-carbon strategy, as well as the Sustainable Development Goals.

Academic Editor: Shicheng Li

Received: 14 August 2025
Revised: 25 September 2025
Accepted: 28 September 2025
Published: 29 September 2025

Citation: Zhao, Y.; Ning, S.; Yan, A.; Jiang, P.; Ren, H.; Li, N.; Huo, T.; Sheng, J. Analysis of Carbon Emissions and Ecosystem Service Value Caused by Land Use Change, and Its Coupling Characteristics in the Wensu Oasis, Northwest China. *Agronomy* **2025**, *15*, 2307. https://doi.org/10.3390/agronomy15102307

Keywords: land use carbon emissions; cultivated land; spatial autocorrelation; PLUS model; remote sensing; sensitivity analysis

1. Introduction

Oases, as distinctive landscapes in arid regions, play a pivotal role in ensuring food security and serve as ecological barriers [1]. The ecosystem services they provide—such as cotton and grain production and water conservation—are vital for sustaining regional socioeconomic development and ecological stability [2,3]. The ecosystem service value (ESV) generated by oasis ecosystems is directly influenced by the extent of cultivated land and crop yields [4]. In recent decades, the drive for large-scale agricultural expansion in oases has intensified human disturbances to the land surface, leading to significant land use/cover changes (LUCCs) and alterations in the regional water–carbon balance [5]. On one hand, the reclamation of cultivated land, expansion of urban and industrial areas, and degradation of forests and grasslands have reshaped the spatial pattern of carbon sources and sinks, weakening carbon sequestration capacity [6,7]. On the other hand, hydrological changes—such as accelerated glacier retreat and wetland shrinkage—have reduced the water-regulating capacity of agricultural systems and impaired their carbon sequestration functions [8,9]. Investigating the spatial interactions between carbon emissions and ESV under LUCC in agriculture-dominated oases is therefore essential for coordinating the water–carbon balance, optimizing agroforestry resource allocation, and developing synergistic strategies for climate change mitigation and adaptation.

In recent years, considerable progress has been made in understanding the impacts of oasis land use change on carbon emissions and ESV. In the field of land use-related carbon emissions, many studies have primarily focused on carbon accounting and its mechanisms [10,11], the effects of carbon emission intensity [12,13], and influencing factors [14,15] across various spatial scales, such as the national [16], provincial [17], and municipal levels [18]. Regarding the influence of land use change on ESV, key areas of study include spatiotemporal evolution patterns [19,20], identification of driving mechanisms [21], ecological zoning frameworks [22], and scenario-based simulations and predictions [23]. Zhang et al. [24] examined the spatiotemporal relationship between land use-related carbon emissions and ESV in the Guanzhong urban agglomeration from 2010 to 2020, revealing a significant negative correlation. Lang et al. [25] investigated the spatiotemporal relationship between carbon emissions and ESV across ecological function zones in Guangdong Province from 2000 to 2020. Their results indicated a positive correlation between carbon emissions and ESV in agricultural production zones. Based on land use data from 2000 to 2020, Chen et al. [26] explored the spatial correlation and driving factors between county-level carbon emissions and ESV in the Yellow River Basin, and proposed policy suggestions for optimizing land use and enhancing ESV. At the international level, policy-oriented studies have also emphasized the connections between land use, carbon sinks, and ecosystem restoration. For example, Dhawi et al. [27] demonstrated that revitalizing oasis agriculture can enhance carbon sequestration and climate resilience, while Kalfas et al. [28] highlighted the importance of integrating land use planning, water resources, and global climate change. However, most studies have examined either carbon emissions or ESV separately, often at national, provincial, or urban scales, without explicitly addressing their coupled dynamics. In addition, few studies or models have combined retrospective analysis with scenario-based simulations to assess how future land use trajectories may influence the carbon–ESV relationship. As a result, research on the coupling mechanisms between

carbon processes and ESV in agricultural oases in arid regions remains scarce [27,29], which hinders sustainable development in these regions.

As a core production base for cotton, grain, and fruit in southern Xinjiang, the Wensu Oasis exemplifies the vulnerability of glacier–river–farmland composite systems. This region relies on glacier meltwater to sustain intensive irrigated agriculture and, over the past three decades, cropland expansion combined with the shrinkage of water bodies has triggered significant ecological effects, severely impacting the oasis's ecological environment and long-term sustainability [30]. In light of these challenges, the Wensu Oasis was taken as a typical study area in northwest China to analyze spatiotemporal variations in land use, carbon emissions, and ESV from 1990 to 2020, and to predict future changes under different development scenarios. The objective of this study is to clarify how LUCC has shaped the coupled dynamics of carbon emissions and ESV in the past three decades in Wensu Oasis, and to predict how these interactions may evolve under alternative land use pathways in the future. The study integrates remote sensing data, carbon emission accounting, ESV estimation, spatial autocorrelation, coupling coordination degree model, and the PLUS model into a comprehensive framework that connects LUCC-driven carbon–ESV interactions historical dynamics with scenario-based prediction and evaluation. This provides practical guidance for balancing agricultural production and ecological protection in the oasis of the arid region, supporting China's dual-carbon strategy and the Sustainable Development Goals.

2. Materials and Methods

2.1. Study Area

The Wensu Oasis (40°51′–42°15′ N, 79°27′–81°29′ E) is recognized by the United Nations as a high-quality production base for "green food" rice. It also serves as a national high-quality cotton production base, the "hometown of walnuts" in China, and a key region for producing the renowned "Bingtangxin" apples. As an important agricultural and pastoral production base and ecological barrier in southern Xinjiang, the oasis is located on the southern slope of the central Tianshan Mountains in western Xinjiang, at the southern foot of Tomur Peak and the northern edge of the Tarim Basin (Figure 1).

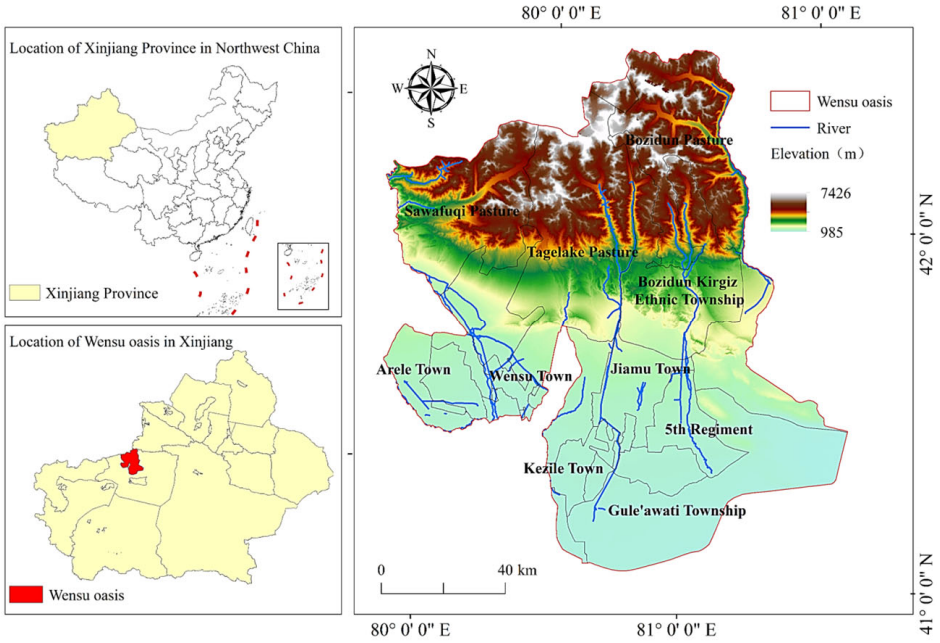

Figure 1. Map of the location of Wensu Oasis in Xinjiang, China.

The region has a population of approximately 2.66×10^5 and a total area of 1.43×10^4 km^2. The plain area in the southern part of the Wensu Oasis accounts for 46.33% of the total area, while the mountainous area in the north accounts for 56.67%. The western part consists mainly of the alluvial plains of the Kumalak and Tushgan Rivers, while the eastern part is dominated by the alluvial plains of the Tailan and Karayulgun Rivers. The oasis is rich in natural resources and features a diverse landscape that integrates multiple ecosystem types, including glaciers, rivers, farmland, grasslands, and deserts. The region exhibits significant vertical topographic variation and has a typical continental arid climate characterized by low precipitation, abundant water resources from rivers and snowmelt, intense evaporation, high solar radiation, and large diurnal temperature differences. The mean annual temperature ranges from 8.4 °C to 10.1 °C, and the annual sunshine duration ranges from 2556 to 2760 h.

2.2. Data Sources

Remote sensing images from Landsat TM/ETM+/OLI for 1990, 2000, 2010, and 2020, with a spatial resolution of 30 m × 30 m, were selected for this study. After preprocessing procedures such as cloud removal, image fusion, and clipping, the land resources in the study area were classified into six categories—forest, grassland, water (including glaciers), cultivated land, construction land, and unused land—based on the National Land Use/Cover Classification System for Remote Sensing Monitoring. Land use classification was conducted using a combination of visual interpretation and supervised classification methods. The classification accuracy of the 2020 land use types was verified through field surveys, yielding an overall accuracy greater than 80%.

The PLUS model was used to simulate land use changes. Based on the specific conditions of the study area and data availability, this study selected socioeconomic factors, distance factors, and meteorological and environmental factors as the driving forces of land use change in the PLUS model (Table 1). These three categories of driving forces were further divided into 12 specific driving factors. The socioeconomic factors include population and GDP; the distance-related factors consist of distances to primary roads, secondary roads, tertiary roads, the county government, and water, all of which were calculated using Euclidean distance; and the meteorological and environmental factors include soil type, annual average precipitation, annual average temperature, digital elevation model (DEM), and slope data. Land use type data and the 12 driving factors were preprocessed through operations such as clipping, resampling, and prediction transformation. All data were standardized to a spatial resolution of 1 km × 1 km with consistent row and column numbers, coordinate system, and prediction type to ensure compatibility for subsequent land use in the PLUS model.

Table 1. Data sources.

Category	Name	Spatial Resolution	Source
Land Use Data	Land use types (1990, 2000, 2010, 2020)	30 m	Geospatial Data Cloud (https://www.gscloud.cn/, accessed on 4 April 2024)
Socioeconomic Data	Population GDP	1 km	Resource and Environment Science and Data Center (https://www.resdc.cn/, accessed on 10 July 2024)
Distance Data	Distance to primary roads Distance to secondary roads Distance to tertiary roads Distance to county government Distance to water	/	National Geomatics Information Center (https://www.webmap.cn/, accessed on 15 July 2024)

Table 1. *Cont.*

Category	Name	Spatial Resolution	Source
Climate and Environmental Data	Soil type Annual average precipitation Annual average temperature	1 km	Resource and Environment Science and Data Center (https://www.resdc.cn/, accessed on 10 July 2024)
	Elevation (DEM) Slope	30 m	Geospatial Data Cloud (https://www.gscloud.cn/, accessed on 4 April 2024)

2.3. Methods

The research framework is illustrated in Figure 2. First, the spatiotemporal distribution characteristics of land use/cover change (LUCC) in the Wensu Oasis from 1990 to 2020 were analyzed. Then, carbon emissions and ESV were calculated using the carbon emission coefficient method and the modified equivalent factor method, respectively, and their spatiotemporal evolution patterns were assessed. Subsequently, spatial autocorrelation analysis and the coupling coordination degree model were employed to investigate the spatiotemporal interactions between carbon emissions and ESV. Finally, the PLUS model was used to simulate LUCC in the oasis under four development scenarios for 2030, 2040, and 2050. Based on the simulation results, the spatiotemporal interaction patterns of carbon emissions and ESV under the four scenarios were analyzed, and corresponding land use regulation strategies were proposed for different cluster regions.

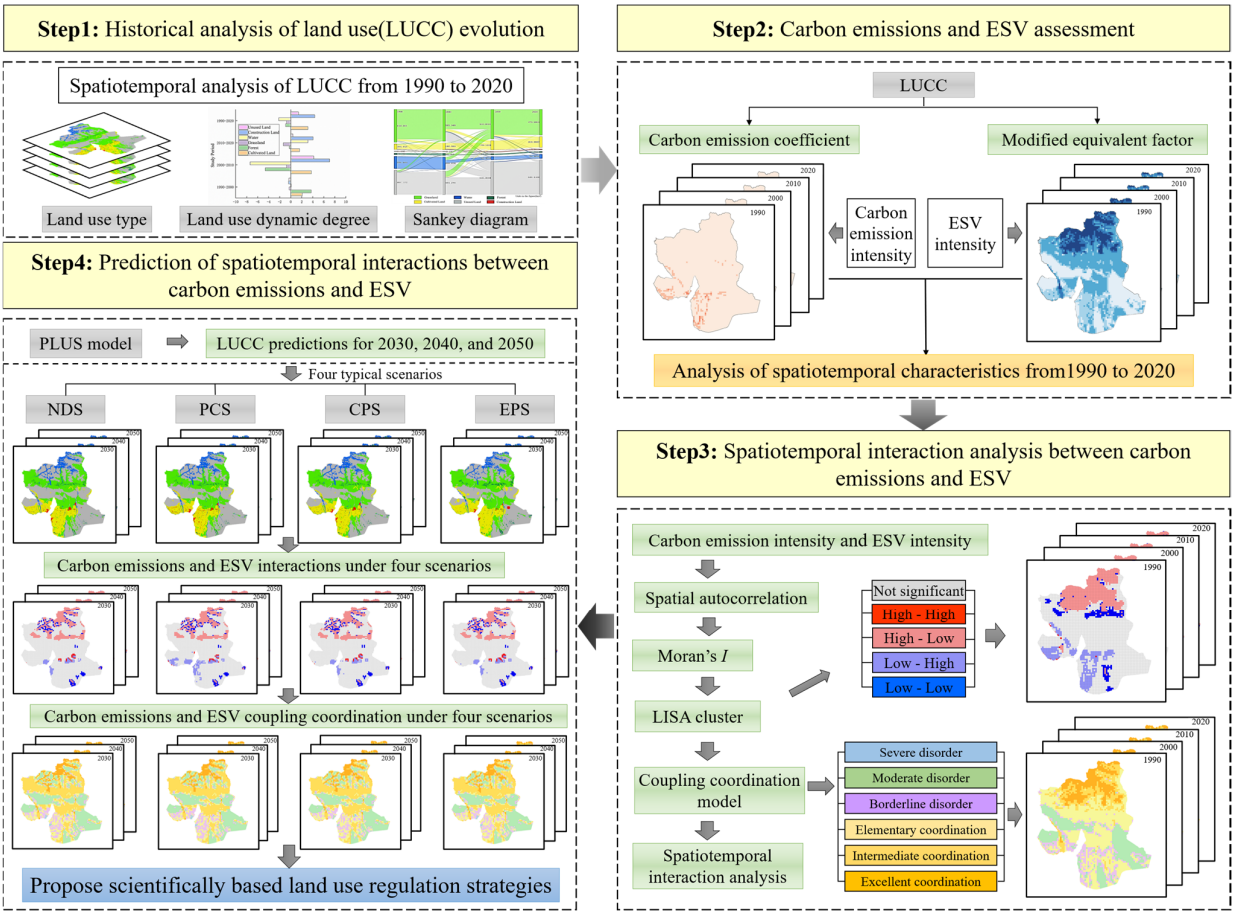

Figure 2. Research flowchart.

2.3.1. Spatiotemporal Dynamics of Land Use Change

The spatiotemporal characteristics of land use in the study area in 1990, 2000, 2010, and 2020 were analyzed using the land use dynamic degree (K) and the land use transfer matrix. The calculation formulas can be found in [31].

2.3.2. Estimation of Land Use Carbon Emissions

The carbon emissions of each land use type were estimated based on the analysis of land use area for different categories in 1990, 2000, 2010, and 2020 in Wensu Oasis. The carbon emission coefficient method [32] was applied to calculate land use carbon emissions. Among them, the carbon emissions of cultivated land, forest, grassland, water, and unused land were calculated using the direct carbon emission coefficient method, while construction land was estimated using the indirect carbon emission coefficient method. The calculation methods are as follows:

(1) Direct Carbon Emission Coefficient Method

$$E = \sum e_k = \sum A_k \times Q_k \tag{1}$$

where E is the total direct carbon emissions (t), A_k is the area of the k-th land use type (hm^2), and Q_k is the carbon emission coefficient of the k-th land use type. According to previous studies [33,34], the carbon emission (or absorption) coefficients for cultivated land, forest, grassland, water, and unused land are 0.442, −0.644, −0.021, −0.253, and −0.005 ($t \cdot hm^{-2}$), respectively.

(2) Indirect Carbon Emission Coefficient Method

$$E_c = \sum E_j \times f_j \tag{2}$$

where E_c is the total carbon emissions from construction land (t), E_j is the consumption of the j-th type of energy (t), and f_j is the carbon emission coefficient of the j-th type of energy. Based on the IPCC Guidelines and relevant literature [34,35], the carbon emission coefficients (in standard coal equivalent) for coal, oil, and natural gas are 0.7488, 0.583, and 0.444 ($t \cdot t^{-1}$), respectively.

The intensity of land use carbon emissions depends on the area of each land use type within the grid and its corresponding carbon emission coefficients. A higher intensity indicates greater carbon emissions. The calculation is as follows:

$$C = \sum \frac{S_i P_i}{S} \tag{3}$$

where C is the carbon emission intensity of land use, S is the total area of the grid cell, and S_i and P_i are the area and carbon emission coefficient of land use type i within the grid, respectively.

2.3.3. Estimation of Ecosystem Service Value

The calculation of ESV includes four categories: provisioning services (food production, raw material production, and water supply), regulating services (gas regulation, climate regulation, waste treatment, and water regulation), supporting services (soil formation, nutrient cycling, and biodiversity maintenance), and cultural services (esthetic landscape). Referring to relevant studies [36,37], this study adopted a modified equivalent factor method to estimate the ESV of the Wensu Oasis. Based on the actual conditions of the study area, the unit values of 11 ecosystem services corresponding to five main LUCC types (cultivated land, forest, grassland, water, and unused land) were adjusted. According

to the principle that the value of one standard equivalent factor equals one-seventh of the economic value of grain yield per unit area of cultivated land, the data on sowing area, yield per unit area, and unit price of major crops in Wensu Oasis were collected, and their averages were calculated. The ecosystem service value was calculated as follows:

$$ESV = \sum_{k=1}^{m} A_k \times VC_k \quad (4)$$

where ESV is the total ecosystem service value (CNY), and VC_k is the unit area value of the ecosystem services for land use type k (CNY·hm^{-2}).

The ecosystem service value intensity ($\overline{ESV}$) provides a visual representation of the spatial distribution of ESV across different regions. It was calculated as follows:

$$\overline{ESV} = \frac{ESV}{S} \quad (5)$$

The ecosystem service value coefficients of different land use types in Wensu Oasis are shown in Table 2.

Table 2. Ecosystem service value coefficients for different land use types in Wensu Oasis from 1990 to 2020 (unit: CNY·hm^{-2}).

Category	Ecosystem Service	Cultivated Land	Forest	Grassland	Water	Unused Land
Provisioning services	Food production	1124.22	256.89	237.39	444.26	5.09
	Raw material production	249.26	590.09	349.31	247.57	15.26
	Water supply	−1327.70	305.22	193.30	4422.27	10.17
Regulating services	Gas regulation	905.48	1940.68	1227.66	966.52	66.13
	Climate regulation	473.09	5806.78	3245.49	2180.61	50.87
	Environmental purification	137.35	1701.59	1071.66	3157.31	208.57
	Hydrological regulation	1521.00	3799.97	2377.31	45,307.96	122.09
Supporting services	Soil retention	529.04	2362.90	1495.57	1098.79	76.30
	Nutrient cycling	157.70	180.59	115.30	84.78	5.09
	Biodiversity maintenance	172.96	2151.79	1359.92	3537.14	71.22
Cultural services	Esthetic landscape	76.30	943.63	600.26	2275.57	30.52
Total	/	4018.71	20,040.12	12,273.17	63,722.79	661.31

Water-related ESV coefficients were adopted from the nationally recognized equivalent factor system and locally adjusted to the oasis context. In Xinjiang, water bodies provide multiple critical services (irrigation supply, hydrological regulation, habitat maintenance); therefore, per-unit ESV for water is higher than for terrestrial covers, consistent with regional applications in the Tarim Basin and Xinjiang [38,39].

2.3.4. Bivariate Spatial Autocorrelation Analysis

Bivariate Moran's I (including global and local bivariate Moran's I) was used to quantify the spatial clustering and dispersion between carbon emission intensity and $\overline{ESV}$ in the oasis area [40]. The global bivariate Moran's I examines whether there is a spatial correlation between carbon emission intensity and $\overline{ESV}$, as well as the degree of

this correlation. The local bivariate Moran's I reveals spatial correlations at specific spatial grids. The bivariate LISA cluster map visualizes local spatial correlations, illustrating the relationship between carbon emission intensity at a given location and the $\overline{ESV}$ of neighboring locations at a certain significance level. The four quadrants generated by bivariate LISA represent four types of local spatial autocorrelations.

2.3.5. Coupling Coordination Degree Model

A coupling coordination degree model was employed to quantify the coordination between land use carbon emissions and ESV [41]. The calculation formula is as follows:

$$D = \sqrt{\frac{2(\alpha U_1 + \beta U_2)\sqrt{U_1 U_2}}{(U_1 + U_2)}} \quad (6)$$

where D represents the coupling coordination degree, with $D \in [0, 1]$; a higher value indicates better coordination between the systems. U_1 and U_2 are the standardized values of land use carbon emission intensity and $\overline{ESV}$, respectively. α and β are coefficients to be determined. Since carbon emissions and ESV are considered equally important in this study, both coefficients are set to $\alpha = \beta = 0.5$. The classification thresholds of the coupling coordination degree (D, with a value range of 0–1) were determined according to established criteria [42] without modification. Specifically, $0 < D \leq 0.2$, $0.2 < D \leq 0.4$, $0.4 < D \leq 0.5$, $0.5 < D \leq 0.6$, $0.6 < D \leq 0.8$, and $0.8 < D \leq 1.0$ represent severe disorder, moderate disorder, borderline disorder, elementary coordination, intermediate coordination, and excellent coordination, respectively.

2.3.6. Land Use Change Simulation

The Patch-generating Land Use Simulation (PLUS) model [43] was employed to simulate land use changes in the oasis and to analyze future variations in land use as well as the resulting changes in carbon emission intensity and $\overline{ESV}$. Using land use data collected for Wensu Oasis in 2000 and 2010, a Markov chain model was used to predict the quantity of different land use types in 2020. The land expansion module was then used to extract land expansion data from 2000 to 2010. Based on the driving factors and land expansion data, the Land Expansion Analysis Strategy (LEAS) module was applied to calculate the suitability probabilities for each land use type. By setting neighborhood weights and transition rules, the CARS module was used to generate simulated land use results for 2020 in Wensu Oasis. Neighborhood weights reflect the expansion ability of different land use types. Since the amount of area change in each land use type over the same spatial and temporal scale can effectively represent the expansion capacity, this study determined the neighborhood weight of each land use type based on the proportion of its expansion area relative to the total land expansion [44].

Based on previous studies [43,45] and taking into full consideration the current land use status and development trends of the Wensu Oasis, four future development scenarios were established: the natural development scenario (NDS), production and construction scenario (PCS), cultivated land protection scenario (CPS), and ecological protection scenario (EPS).

The Wensu Oasis is located in the arid region of the northwest inland, where water resources are scarce and cultivated land is a valuable asset. Thus, in all four scenarios, the conversion of water to any other land use type is prohibited. In the PCS, cultivated land is restricted from being converted into any land use type other than construction land, and construction land is prohibited from being converted into any other type. In the CPS, the conversion of cultivated land into other land use types is limited. In the EPS, the probability of converting cultivated land and construction land to grassland is increased by

40%, while the probability of converting them to forest is increased by 20%. Additionally, the probability of converting grassland to forest is increased by 40%. In the transition matrix (Table 3), cultivated land, forest, grassland, water, construction land, and unused land are represented by *a*, *b*, *c*, *d*, *e*, and *f*, respectively. A value of 0 indicates that conversion is not allowed, while 1 indicates that conversion is permitted.

Table 3. Parameters for the land use transition matrix under different scenarios.

Type	Natural Development Scenario (NDS)						Production and Construction Scenario (PCS)						Cultivated Land Protection Scenario (CPS)						Ecological Protection Scenario (EPS)					
	a	**b**	**c**	**d**	**e**	**f**	**a**	**b**	**c**	**d**	**e**	**f**	**a**	**b**	**c**	**d**	**e**	**f**	**a**	**b**	**c**	**d**	**e**	**f**
a	1	1	1	1	1	1	1	0	0	0	1	0	1	1	1	1	1	1	1	1	1	1	1	1
b	1	1	1	1	1	1	1	1	1	1	1	1	1	1	1	1	1	1	1	1	1	1	1	1
c	1	1	1	1	1	1	1	1	1	1	1	1	1	1	1	1	1	1	1	1	1	1	1	1
d	0	0	0	1	0	0	0	0	0	1	0	0	0	0	0	1	0	0	0	0	0	1	0	0
e	1	1	1	1	1	1	0	0	0	0	1	0	0	1	1	1	1	1	1	1	1	1	1	1
f	1	1	1	1	1	1	1	1	1	1	1	1	1	1	1	1	1	1	1	1	1	1	1	1

2.3.7. Sensitivity Analysis

The sensitivity index (Coefficient of Sensitivity, *CS*) was employed to test the reliability of the ecosystem service function evaluation results. This index is used to verify the extent to which the estimated ecosystem service value depends on the value coefficients of ecosystem service functions [46].

$$CS = \left| \frac{(ESV_j - ESV_i)/ESV_i}{(E_k - E_i)/E_i} \right| \quad (7)$$

where ESV_i and ESV_j represent the ecosystem service values before and after adjustment, respectively, while E_i and E_k denote the equivalent coefficients of ecosystem service functions before and after adjustment. A *CS* greater than 1 indicates the ESV is elastic, whereas a *CS* less than 1 suggests that the ESV is inelastic, implying that the results are more reliable.

3. Results

3.1. Spatiotemporal Characteristics of Land Use in Wensu Oasis

Figure 3 illustrates the variations in the land use dynamic degree (*K*) in the Wensu Oasis during different time periods. From 1990 to 2000, the areas occupied by water ($K = 0.09\%$), cultivated land ($K = 2.10\%$), and forests ($K = 3.71\%$) increased, while the areas occupied by grassland ($K = -0.30\%$), construction land ($K = -0.38\%$), and unused land ($K = -0.35\%$) decreased, indicating an improvement in local awareness of natural resource conservation. The significant increase in forest area may be attributed to afforestation projects or ecological policies implemented during this period. Between 2000 and 2010, grassland ($K = -0.74\%$), forest ($K = -4.61\%$), and water ($K = -7.38\%$) areas experienced a notable decline, suggesting mounting challenges in water resource conservation; in contrast, cultivated land ($K = 3.75\%$), unused land ($K = 4.17\%$), and construction land ($K = 7.05\%$) expanded, reflecting an acceleration of urbanization in the region. From 2010 to 2020, unused land ($K = 0.39\%$), cultivated land ($K = 1.61\%$), water area ($K = 3.11\%$), and construction land ($K = 4.06\%$) continued to expand, although at a slower pace; meanwhile, grassland ($K = -1.34\%$) and forest land ($K = -0.26\%$) kept shrinking. Overall, in the past three decades, areas occupied by unused land ($K = 1.41\%$), cultivated land ($K = 3.11\%$), and construction land (with the highest increase, $K = 4.35\%$) expanded steadily, whereas grassland ($K = -0.74\%$), forests ($K = -0.93\%$), and water areas ($K = -2.18\%$) declined. These

trends suggest that while the region has experienced rapid socioeconomic development, the intensity of ecological protection remains insufficient and needs further enhancement.

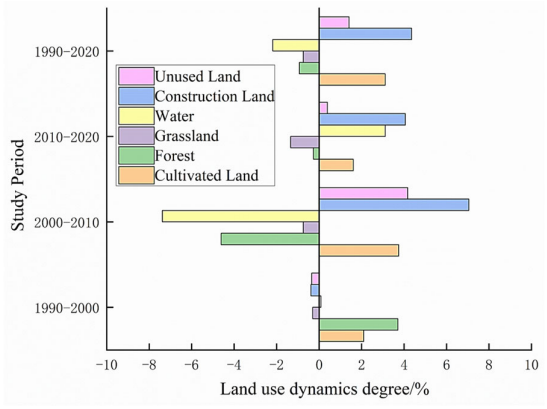

Figure 3. Land use dynamics degree in Wensu Oasis from 1990 to 2020.

Analysis of land use type conversion in Wensu Oasis from 1990 to 2020 (Figure 4) reveals a significant increase in unused land, with a total inflow of 3157.32 km^2. The majority of this increase originated from grassland (1815.37 km^2, accounting for 57.5%) and water area (1318.76 km^2, accounting for 41.8%). During the same period, 1257.96 km^2 of unused land was converted to other types, mainly grassland (960.46 km^2, 76.4% of the total outflow) and cultivated land (224.65 km^2, 17.9%). Grassland showed a clear decreasing trend, with a total inflow of 1453.85 km^2, primarily from unused land (67.0%), followed by forest and water areas. The outflow of grassland reached 2817.78 km^2, mainly to cultivated land and unused land. Cultivated land exhibited an increasing trend, with a total inflow of 1145.38 km^2, primarily from grassland and unused land, while the outflow was relatively small (170.82 km^2). Water experienced a significant net loss, with a total outflow of 1605.12 km^2, of which 82.0% was converted to unused land. The inflow was only 106.29 km^2. The converted forest and construction lands were relatively small. Forests saw an inflow of 137.19 km^2 and an outflow of 215.11 km^2. Construction land had an inflow of 101.65 km^2, mainly from cultivated land (64.37 km^2, 63.33%), and an outflow of 34.88 km^2, primarily to cultivated land (30.77 km^2).

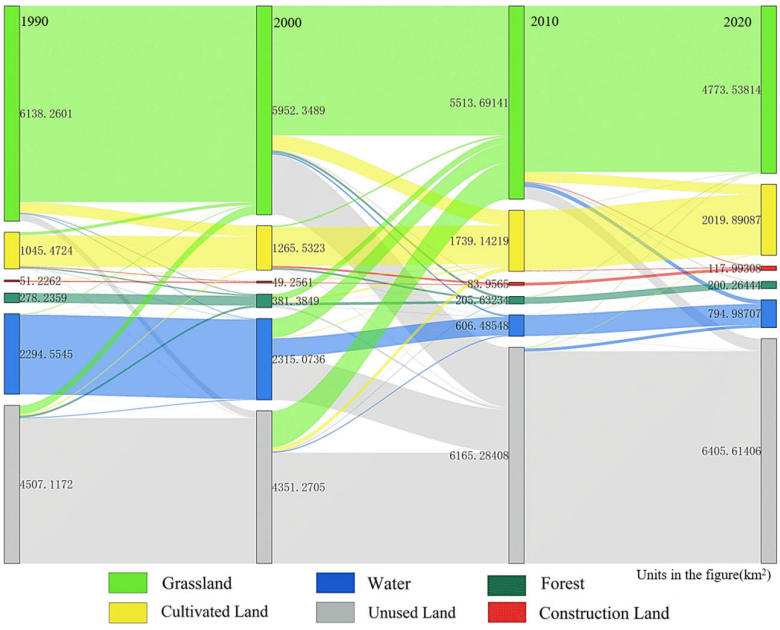

Figure 4. Sankey diagram of land use transition matrix in Wensu Oasis from 1990 to 2020.

The results reflect the general land use change characteristics in the Wensu Oasis between 1990 and 2020, marked by the expansion of unused land, a reduction in grassland, and the growth of cultivated land. The patterns of land use conversion in the periods 1990–2000, 2000–2010, and 2010–2020 were largely consistent with those observed over the entire 1990–2020 period.

3.2. Spatiotemporal Characteristics of Land Use Carbon Emissions in Wensu Oasis

3.2.1. Temporal Characteristics of Land Use Carbon Emissions

Land use change and land utilization intensity have a significant influence on land use carbon emissions. Based on Equations (1) and (2), the carbon sources, carbon sinks, and net carbon emissions in Wensu Oasis for the years 1990, 2000, 2010, and 2020 are shown in Table 4. The carbon source (carbon emissions) from land use increased from 23.90 $\times$ 10^4 t in 1990 to 169.17 $\times$ 10^4 t in 2020. The average annual growth rates of carbon emissions for the periods 1990–2000, 2000–2010, 2010–2020, and 2000–2020 were 5.45%, 15.52%, 7.95%, and 20.26%, respectively. Among land use types, carbon emissions from construction land increased rapidly, rising from 19.28 $\times$ 10^4 t in 1990 to 160.24 $\times$ 10^4 t in 2020. The corresponding average annual growth rates were 6.25%, 17.63%, 8.51%, and 24.37%. In contrast, carbon emissions from cultivated land increased more gradually, from 4.62 $\times$ 10^4 t in 1990 to 8.93 $\times$ 10^4 t in 2020, with average annual growth rates of 2.10%, 3.77%, 1.61%, and 3.11%, respectively.

Table 4. Carbon emissions by land use type in Wensu Oasis from 1990 to 2020.

Year	Carbon Source/$\times 10^4$ t			Carbon Sink/$\times 10^4$ t					Net Carbon Emissions /$\times 10^4$ t
	Cultivated Land	Construction Land	Total	Forest	Grassland	Water	Unused Land	Total	
1990	4.62	19.28	23.90	−1.79	−1.29	−5.81	−0.23	−9.11	14.78
2000	5.59	31.33	36.93	−2.46	−1.25	−5.86	−0.22	−9.78	27.15
2010	7.69	86.55	94.24	−1.32	−1.16	−1.54	−0.31	−4.33	89.91
2020	8.93	160.24	169.17	−1.29	−1.00	−2.01	−0.32	−4.63	164.55

The carbon sink (carbon absorption) in Wensu Oasis declined from 9.11 $\times$ 10^4 t in 1990 to 4.63 $\times$ 10^4 t in 2020, with an average annual decrease of 0.15 $\times$ 10^4 t, corresponding to a mean annual decline rate of 1.64%. From 1990 to 2000, the carbon sink exhibited an average annual increase of 0.74%, followed by a decline of 5.57% in 2000–2010, and a slight rebound with an average annual increase of 0.69% in 2010–2020. Among all land use types, water contributed the most to carbon sinks, accounting for 63.78%, 59.92%, 35.57%, and 43.41% of the total carbon sink in 1990, 2000, 2010, and 2020, respectively. Grassland contributed the least, accounting for 14.16%, 12.78%, 26.79%, and 21.60%, respectively.

The net carbon emissions in the Wensu Oasis increased continuously from 14.78 $\times$ 10^4 t in 1990 to 164.55 $\times$ 10^4 t in 2020, with an average annual growth rate of 33.78%, closely following the trend of carbon source growth. The average annual growth rates of net carbon emissions were 8.37% in 1990–2000, 23.16% in 2000–2010, 8.31% in 2010–2020, and 33.78% over the entire 1990–2020 period. The continuous expansion of construction land and the associated increase in carbon emissions were the key drivers of the rising net carbon emissions in Wensu Oasis.

3.2.2. Spatial Characteristics of Land Use Carbon Emissions

Carbon emission intensity provides a visual representation of the spatial distribution patterns and characteristics of carbon emissions from land use in the study area. Following relevant studies [26], the Wensu Oasis was divided into 3808 grid units, each measuring 2 km $\times$ 2 km. Using the natural breaks method, the land use carbon emissions in Wensu

Oasis were classified into five levels: I, II, III, IV, and V. The spatial distribution of carbon emission intensity was mapped accordingly (Figure 5).

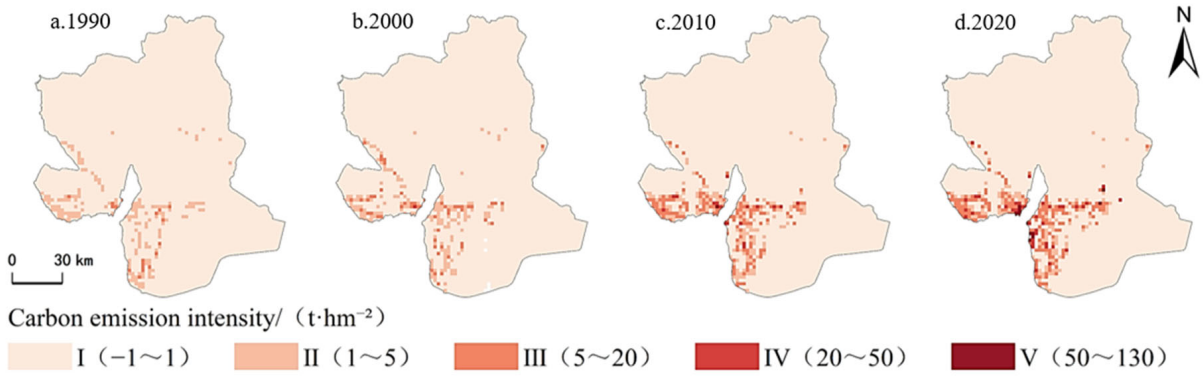

Figure 5. Spatial distribution of carbon emission intensity from land use in Wensu Oasis from 1990 to 2020.

Spatiotemporal variations in land use carbon emission intensity were evident in Wensu Oasis from 1990 to 2020. Overall, the carbon emission intensity remained low, but it gradually increased over time. The maximum carbon emission intensity increased from 10.15 t/hm^2 in 1990 to 129.87 t/hm^2 in 2020, representing a 12.7-fold increase. Level I zones were mainly distributed in the northern, central, and southwestern parts of the oasis, while Level V zones were concentrated in the southern and southwestern areas, indicating a clustered spatial pattern. The Wensu Oasis was predominantly composed of Level I and Level II zones. Although the area covered by Level I zones showed a decreasing trend from 94.81% in 1990 to 90.44% in 2020, it remained dominant. The area covered by Level II zones also declined annually, from 4.70% in 1990 to 3.53% in 2020. The area covered by Level III zones exhibited the largest increase, expanding from 0.49% in 1990 to 4.70% in 2020, followed by Level IV and Level V zones, which were mainly distributed around Level V zones. Notably, Level IV zones showed the most significant temporal variation: no Level IV grids existed in 1990, yet by 2020, they accounted for 1.05% of the total area and were highly correlated with the spatial distribution of construction land.

The expansion of Level IV and V zones in carbon emission intensity was strongly associated with the expansion of construction land. Combined with the analysis in Section 3.1 and Figure 5, it can be seen that the increase in construction land mainly originated from cultivated land, with smaller contributions from grassland and unused land. Overall, cultivated land showed a net conversion-in trend, primarily from grassland and unused land; therefore, it can be inferred that the continuous increase in net carbon emissions in Wensu Oasis was mainly driven by rapid socioeconomic development, which led to the significant expansion of construction land and the increased development of unused land, both of which contributed to higher carbon emissions.

3.3. Spatiotemporal Characteristics of Ecosystem Service Value in Wensu Oasis

3.3.1. Temporal Variation in Ecosystem Service Value

The ecosystem service value (ESV) of Wensu Oasis exhibited a general downward trend from 1990 to 2020 (Figure 6). The total ESV decreased from CNY 234.32 × 10^9 in 1990 to CNY 125.67 × 10^9 in 2020, representing a decline of 46.37%, with an average annual decrease of CNY 3.62 × 10^9. Among the land use types, the ESVs of cultivated land and unused land showed an increasing trend, while those of grassland, forest, and water areas decreased. From 1990 to 2000, the ESV increased by only CNY 1.86 × 10^9. In 2000–2010, the ESV experienced a significant decline, with an average annual decrease of CNY 11.46 × 10^9.

Notably, the ESV of the water area decreased by CNY 108.84 × 10^9, a reduction of 73.78%. The ESV increased slightly between 2010 and 2020, increasing by CNY 4.13 × 10^9. In terms of land use categories, from 1990 to 2020, the ESV of cultivated land and unused land increased by 93.25% and 42.16%, respectively; meanwhile, the ESV of water, forest, and grassland declined, with the largest decrease seen in the water area (65.32%), followed by forest land (28.02%) and grassland (22.23%). These trends are consistent with the land use changes observed in Wensu Oasis.

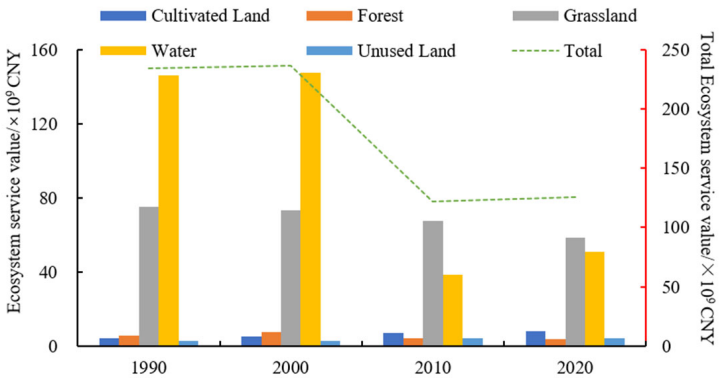

Figure 6. Ecosystem service values by category and their changes in Wensu Oasis from 1990 to 2020.

As shown in Figure 7, the ESVs of all primary ecosystem service categories in Wensu Oasis exhibited a fluctuating downward trend, consistent with the overall trend of the region's total ESV. Among them, the proportion of regulatory services in the total ESV was dominant, accounting for 75.09%, 75.15%, 70.57%, and 72.05% in 1990, 2000, 2010, and 2020, respectively. In contrast, cultural services consistently had the lowest share in all years (≤4.28%). At the secondary service level, the ESV of food production showed an overall increasing trend with fluctuations, while the other ten subcategories exhibited fluctuating declines. This may be attributed to the continuous expansion of cultivated land driven by population growth between 1990 and 2000, which led to increased food production and, consequently, a rise in its service value. In addition, the service value of hydrological regulation experienced a sharp decline over the past 30 years, decreasing by CNY 69.73 × 10^9. The service value of water supply also dropped by CNY 8.19 × 10^9 during the same period. The ESVs of raw material production, gas regulation, climate regulation, environmental purification, soil conservation, nutrient cycling, biodiversity maintenance, and esthetic landscapes all showed a slight increase in 2000, followed by a gradual decline.

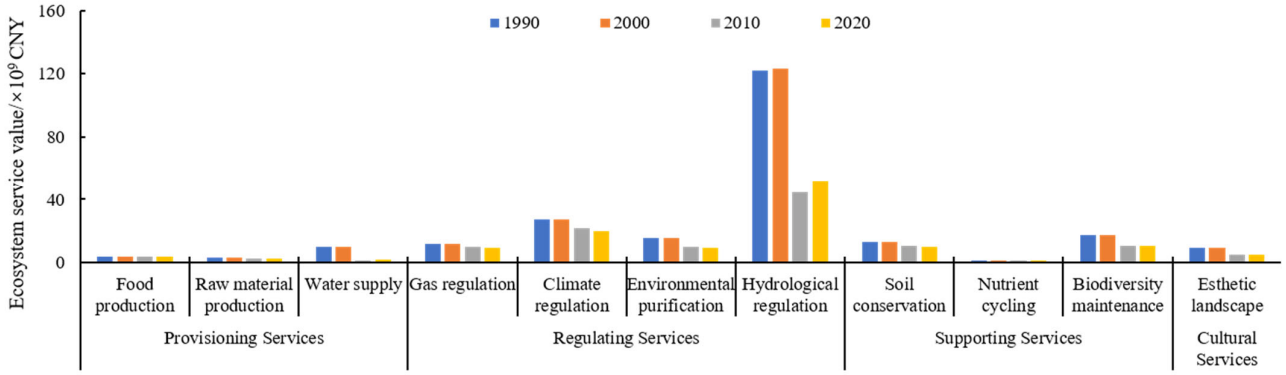

Figure 7. Changes in individual ecosystem service values in Wensu Oasis from 1990 to 2020.

3.3.2. Spatial Distribution Characteristics of Ecosystem Service Value

According to the relevant literature [29], the study area was divided into 2 km × 2 km grid units, resulting in a total of 3808 grids. Using the natural breaks classification method, the ESV of Wensu Oasis was categorized into five levels: I, II, III, IV, and V. The spatial distribution of $\overline{ESV}$ in Wensu Oasis is shown in Figure 8.

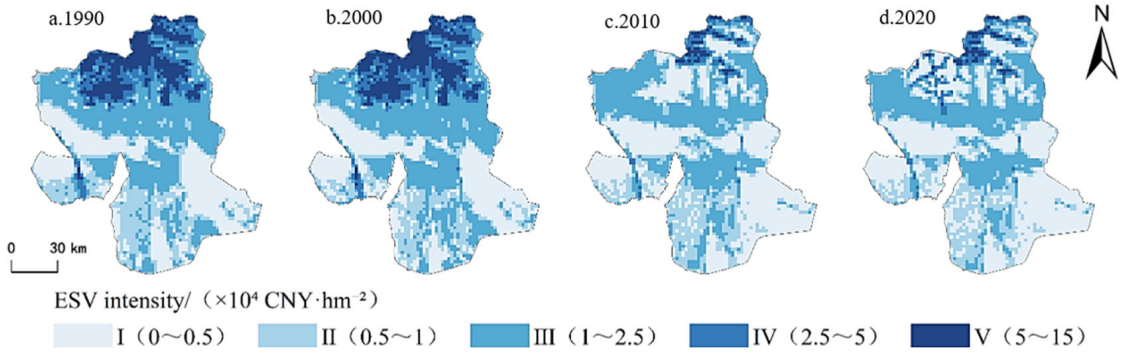

Figure 8. Spatial distribution of ecosystem service value intensity in Wensu Oasis from 1990 to 2020.

The spatial variations in per-unit-area ESV of Wensu Oasis in 1990 are shown in Figure 8. The Level I zone was mainly distributed in the central–western and southeastern parts of the oasis, dominated by unused land. The Level II zone was mainly located in the southern cultivated land areas. The Level III zone was concentrated in the central and northwestern regions, mostly covered by grassland. Level IV and V zones were primarily distributed in the northern mountainous areas and water-rich regions near rivers.

In 2000, the spatial distribution of $\overline{ESV}$ was largely consistent with that in 1990. The proportions of areas covered by Level I, IV, and V zones changed slightly, while those covered by Level II zones decreased by 1.81% and Level III zones increased by 1.65%.

The spatial pattern changed significantly in 2010. Level I zone expanded mainly toward the northern mountainous areas and surrounding unused land, occupying the largest proportion (39.05%). Level II zone accounted for 22.06%, with denser distribution in the southern region due to the expansion of cultivated land in irrigation zones. The distribution of the Level III zone remained relatively stable. Level IV and V zones decreased sharply, particularly in the northern mountainous areas; this may be associated with glacial melt caused by rising temperatures and the conversion of water into unused land. By 2020, the spatial distribution of $\overline{ESV}$ had changed only slightly. Level IV and V zones expanded slightly in the northern part, while Level I, II, and III zones showed similar distributions to those in 2010.

From 1990 to 2020, the $\overline{ESV}$ of Wensu Oasis showed a declining trend. Level I zone accounted for over 25% of the total area and gradually increased over time. Level III zone expanded and then contracted, consistently covering more than 30%. Level IV and V zones shrank significantly between 2000 and 2010 (both <3%), with slight expansion from 2010 to 2020.

3.4. Coupling Characteristics Between Land Use Carbon Emission Intensity and Ecosystem Service Value Intensity from 1990 to 2020

3.4.1. Spatial Correlation

The spatiotemporal distribution characteristics of land use carbon emission intensity and $\overline{ESV}$ of Wensu Oasis revealed that areas with higher carbon emission intensity tended to have lower $\overline{ESV}$, and vice versa (Figures 5 and 8). A potential correlation between carbon emission intensity and $\overline{ESV}$ was postulated, and a correlation analysis was conducted using data from 1990, 2000, 2010, and 2020. The results showed a highly significant

negative correlation between land use carbon emission intensity and $\overline{ESV}$, with correlation coefficients of −0.228, −0.190, −0.089, and −0.080, respectively ($p < 0.01$). Subsequently, a bivariate spatial autocorrelation analysis was performed to further examine the spatial relationship between the two variables. The global Moran's *I* indices for the years 1990, 2000, 2010, and 2020 are presented in Table 5. All Moran's *I* values were negative, with *p*-values less than 0.001 and |z| values greater than 3.29, indicating a highly significant spatial negative correlation between land use carbon emission intensity and $\overline{ESV}$; in other words, areas with higher carbon emission intensity tend to have lower $\overline{ESV}$.

Table 5. Bivariate global Moran's *I* index for Wensu Oasis from 1990 to 2020.

Year	Moran's *I*	*p*	*z*
1990	−0.188	<0.001	−29.779
2000	−0.165	<0.001	−27.713
2010	−0.058	<0.001	−9.845
2020	−0.065	<0.001	−11.035

According to the bivariate LISA cluster map (Figure 9), the spatial correlation between land use carbon emission intensity and $\overline{ESV}$ can be classified into four types: high–high clusters (high ESV–high carbon emissions), high–low clusters (high ESV–low carbon emissions), low–high clusters (low ESV–high carbon emissions), and low–low clusters (low ESV–low carbon emissions). High–high clusters were relatively scarce and scattered, primarily distributed along rivers. These areas exhibited high carbon emissions from surrounding construction land, as well as high ESV due to water conservation services. High–low clusters exhibited a patchy distribution in the northern mountainous areas, where land types mainly included water (glaciers) and forest. With high forest coverage, these areas functioned as carbon sinks and generated high ESV. Low–high clusters were predominantly distributed in patches in the southern and southwestern regions. As urbanization progressed, the expansion of construction land led to increased carbon emissions, thereby reducing ESV. Low–low clusters were mainly located in the central part of the oasis, with a few in the south. These regions had lower levels of economic development, low carbon emissions, and poor ecological conditions, resulting in low ESV.

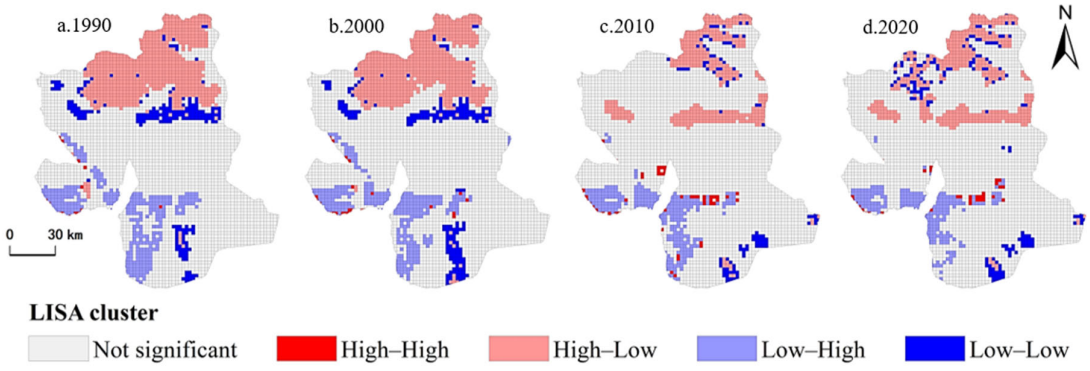

Figure 9. LISA cluster maps of bivariate spatial linkages in Wensu Oasis from 1990 to 2020.

3.4.2. Coupling Coordination Degree

The coupling coordination degree model was used to analyze the coupling coordination relationship between land use carbon emission intensity and $\overline{ESV}$ in the oasis. The results show that from 1990 to 2020, the *D* between land use carbon emission intensity and $\overline{ESV}$ in Wensu Oasis exhibited a declining trend (Figure 10). The average coupling coordination degree decreased from 0.545 in 1990 to 0.514 in 2020. Overall, the oasis showed

a low level of coupling coordination, with a spatial distribution pattern of "higher in the north and lower in the south." Most areas fell into the categories of moderate disorder and intermediate coordination, indicating that the coordinated development between the two systems needs further improvement.

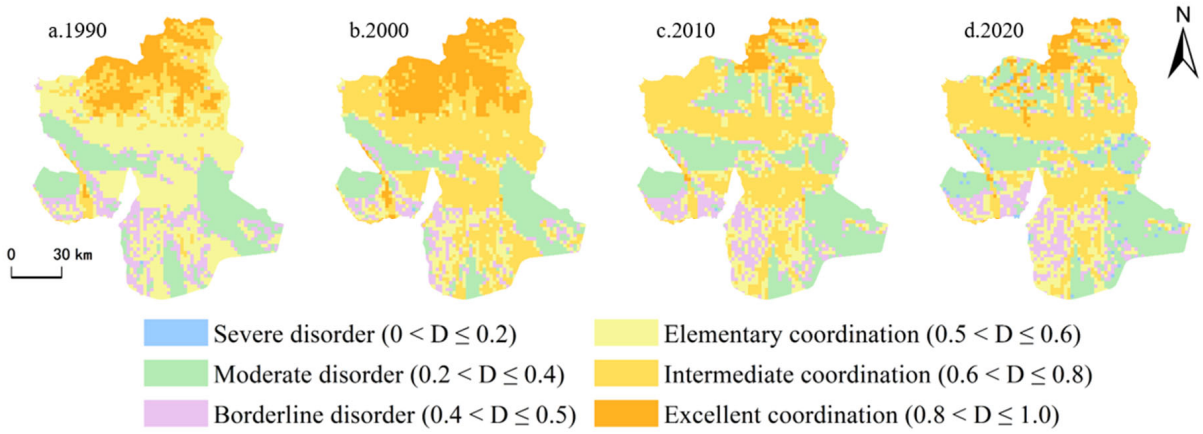

Figure 10. Spatial distributions of coupled coordination types of land use carbon emission intensity and ESV intensity in Wensu Oasis from 1990 to 2020.

In terms of different coupling coordination types, zones of excellent coordination were mainly distributed in the northern mountainous areas but experienced a significant reduction in 2010, with the number of grid cells decreasing from 731 in 2000 to 165 in 2010, a 75% reduction in area. Zones of intermediate coordination were primarily located in the central grasslands and experienced substantial expansion in 2000, with an increase of 1024 grid cells, and remained at a relatively high level thereafter. Zones of elementary coordination were sparsely distributed and saw a significant shift toward intermediate coordination between 1990 and 2000, resulting in a 67% decrease in area. Borderline disorder zones were mainly distributed in southern construction land, with little change in area. Zones of moderate disorder were concentrated in unused land in the central and southern parts of the oasis. In 2010, these areas expanded significantly, with the number of grid cells increasing from 720 in 2000 to 1146 in 2010, an increase of 60%. Zones of severe disorder were relatively limited in distribution.

3.5. Coupling Characteristics Between Land Use Carbon Emission Intensity and Ecosystem Service Value Intensity from 2030 to 2050

3.5.1. Land Use Change Trends Under Multiple Scenarios

The reliability of the land use simulation results for 2020 produced by the PLUS model using land use data from 2000 and 2010 in Wensu Oasis was verified. The resulting Kappa coefficient of 0.86 and overall accuracy of 0.91 indicated that the PLUS model performed well and could accurately reflect land use changes in the study area.

Based on the 2010 and 2020 land use data for Wensu Oasis, the PLUS model was used to project land use trends in 2030, 2040, and 2050 under four scenarios: the natural development scenario (NDS), the production and construction scenario (PCS), the cultivated land protection scenario (CPS), and the ecological protection scenario (EPS). The simulation results are shown in Figures 11 and 12. The projected land use trends under different development scenarios vary as follows: (1) Under the NDS, the cultivated land area continues to expand, while construction land gradually shrinks. Forest land, unused land, grassland, and water show opposing trends, with forest and unused land initially decreasing and then increasing, and grassland and water following the opposite pattern. (2) Under the PCS, grassland experiences a sharp decline compared with 2020, while

construction land reaches its peak area (203.97 km^2). (3) Under the CPS, the expansion rate of cultivated land increases, while the trends for other land use types are generally similar to those in the NDS. (4) Under the EPS, the trend of forest, grassland, and other ecological land types being converted to other land use types is significantly curbed.

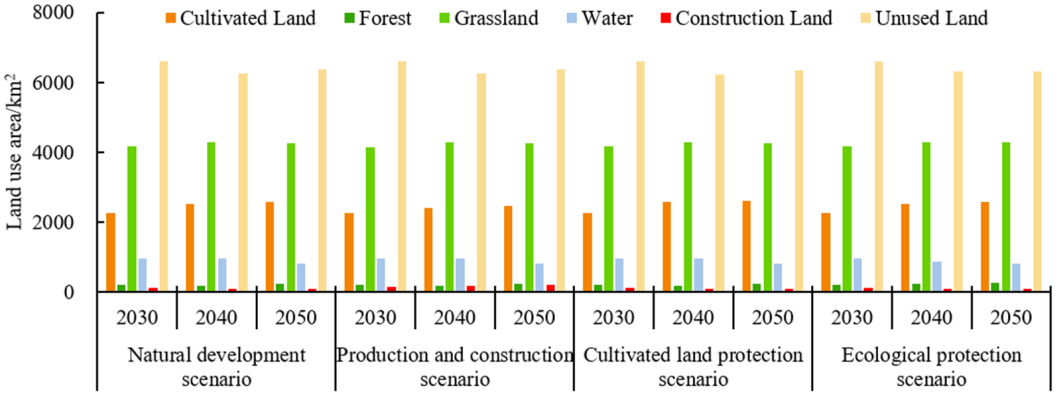

Figure 11. Prediction of land use area in Wensu Oasis under natural development, production and construction, cultivated land protection, and ecological protection scenarios for the years 2030, 2040, and 2050.

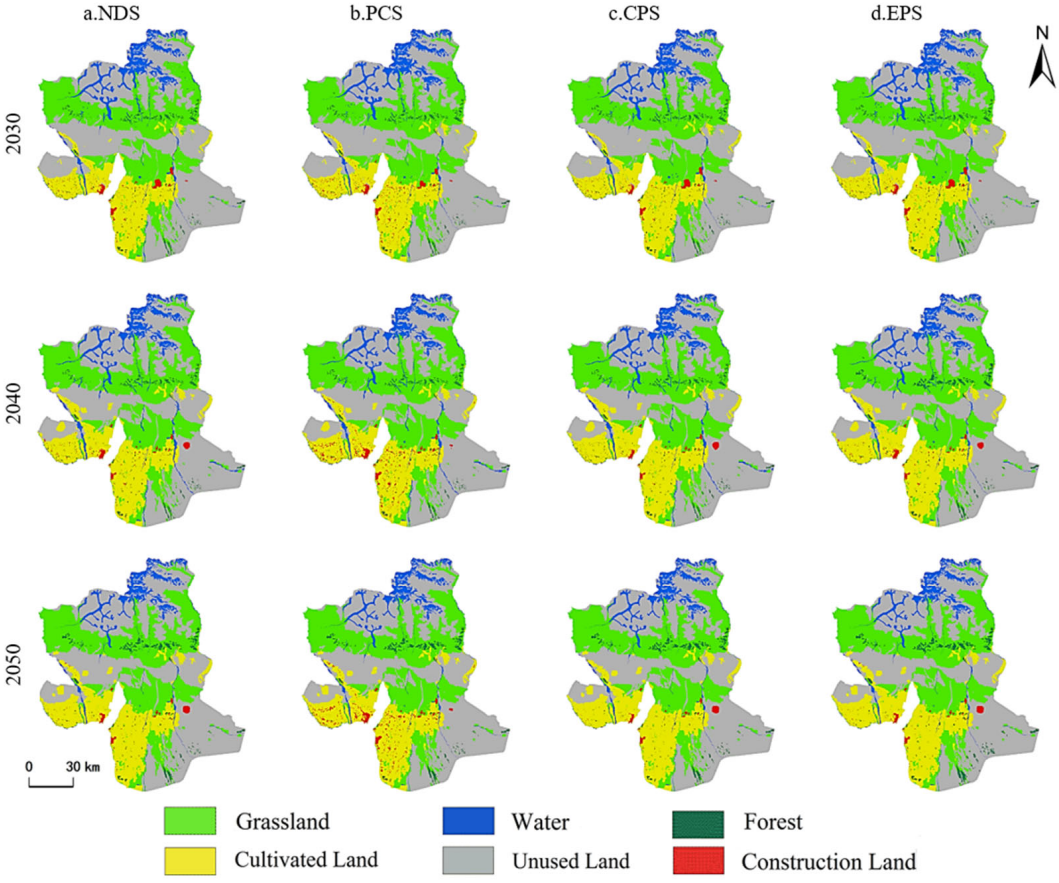

Figure 12. Prediction of land use classification in Wensu Oasis under natural development (**a**), production and construction (**b**), cultivated land protection (**c**), and ecological protection (**d**) scenarios for the years 2030, 2040, and 2050.

3.5.2. Spatial Correlation and Coupling Coordination Degree Under Multiple Scenarios

Based on the predictions of land use for 2030, 2040, and 2050 under the four development scenarios in Wensu Oasis using the PLUS model, the carbon emission intensity

and $\overline{ESV}$ were calculated, and their spatial correlation was analyzed to explore the future relationship between carbon emission intensity and $\overline{ESV}$ in the region. The Moran's I indices under all four scenarios exhibited an overall declining trend from 2030 to 2050, as shown in Table 6, indicating a weakened spatial correlation between land use carbon emission intensity and $\overline{ESV}$ in Wensu Oasis over time.

Table 6. Bivariate global Moran's I index for Wensu Oasis under scenarios of natural development (NDS), production and construction (PCS), cultivated land protection (CPS), and ecological protection (EPS) for the years 2030, 2040, and 2050.

Year	Scenarios	Moran's I	p	z
2030	NDS	−0.0521	<0.001	−8.7067
	PCS	−0.0657	<0.001	−10.9012
	CPS	−0.0509	<0.001	−8.1292
	EPS	−0.0522	<0.001	−8.516
2040	NDS	−0.0609	<0.001	−10.0042
	PCS	−0.0821	<0.001	−12.8477
	CPS	−0.055	<0.001	−9.128
	EPS	−0.0611	<0.001	−10.0111
2050	NDS	−0.0565	<0.001	−9.0101
	PCS	−0.0827	<0.001	−13.9905
	CPS	−0.0538	<0.001	−9.2033
	EPS	−0.0569	<0.001	−9.3634

As shown in Table 7, Figures 13 and 14, under different scenarios for 2030, 2040, and 2050, the bivariate LISA maps of Wensu Oasis are predominantly characterized by High–Low clusters, which appear in patches mainly distributed in the northern part of the oasis. These areas are primarily composed of forest, grassland, and water (glacier). Low–High clusters are the second most common and are mainly concentrated in areas of clustered construction land. The spatial distribution of Low–Low clusters remains largely consistent with that observed in 2020. High–High clusters are the least common and are mainly located in cultivated land (paddy fields) near water systems.

Table 7. Areas of bivariate spatial association types and coupling coordination categories in Wensu Oasis under four scenarios of natural development (NDS), production and construction (PCS), cultivated land protection (CPS), and ecological protection (EPS) for the years 2030, 2040, and 2050 (km^2).

Type	NDS			PCS			CPS			EPS		
	2030	2040	2050	2030	2040	2050	2030	2040	2050	2030	2040	2050
High–High	108.3	82.3	72.6	97.9	124.6	110.6	104.8	86.2	80.5	111.1	79.7	75.4
High–Low	684.1	707.4	619.0	619.8	692.7	633.1	682.8	701.0	601.5	636.8	599.4	652.5
Low–High	392.1	404.2	393.5	728.5	956.6	1018.2	426.8	374.9	390.8	392.4	443.8	403.5
Low–Low	2188.1	2017.4	1952.4	1942.6	2004.8	1956.4	2102.8	2076.8	1957.6	1999.1	1957.4	1878.2
Severe disorder	33.9	33.9	37.6	30.1	33.9	30.1	18.8	26.3	33.9	33.9	33.9	37.6
Moderate disorder	4413.4	4168.8	4195.1	4451.0	4217.7	4236.5	4435.9	4112.4	4146.2	4424.6	4217.7	4108.6
Borderline disorder	1854.9	1869.9	2114.5	2005.4	1971.5	2434.3	1843.6	1903.8	2174.7	1828.6	1971.5	2182.2
Elementary coordination	2329.0	2400.4	2366.6	2178.5	2332.7	2046.8	2351.5	2430.5	2355.3	2329.0	2332.7	2344.0
Intermediate coordination	4541.3	4703.1	4646.6	4514.9	4736.9	4616.5	4533.8	4718.1	4650.4	4556.3	4736.9	4684.3
Excellent coordination	1136.3	1132.5	948.1	1128.7	1015.9	944.4	1125.0	1117.5	948.1	1136.3	1015.9	951.9

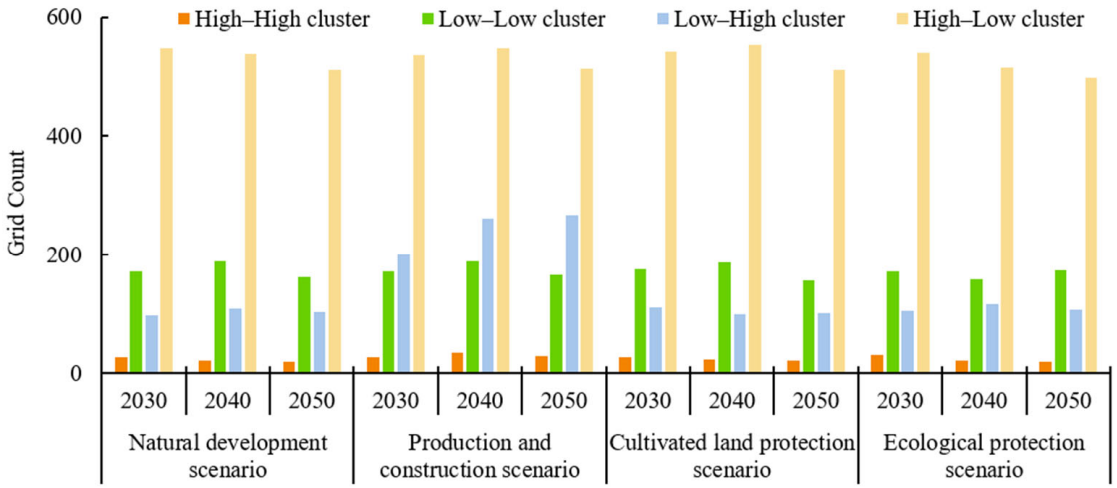

Figure 13. Number of bivariate grid cells for Wensu Oasis under natural development, production and construction, cultivated land protection, and ecological protection scenarios for the years 2030, 2040, and 2050.

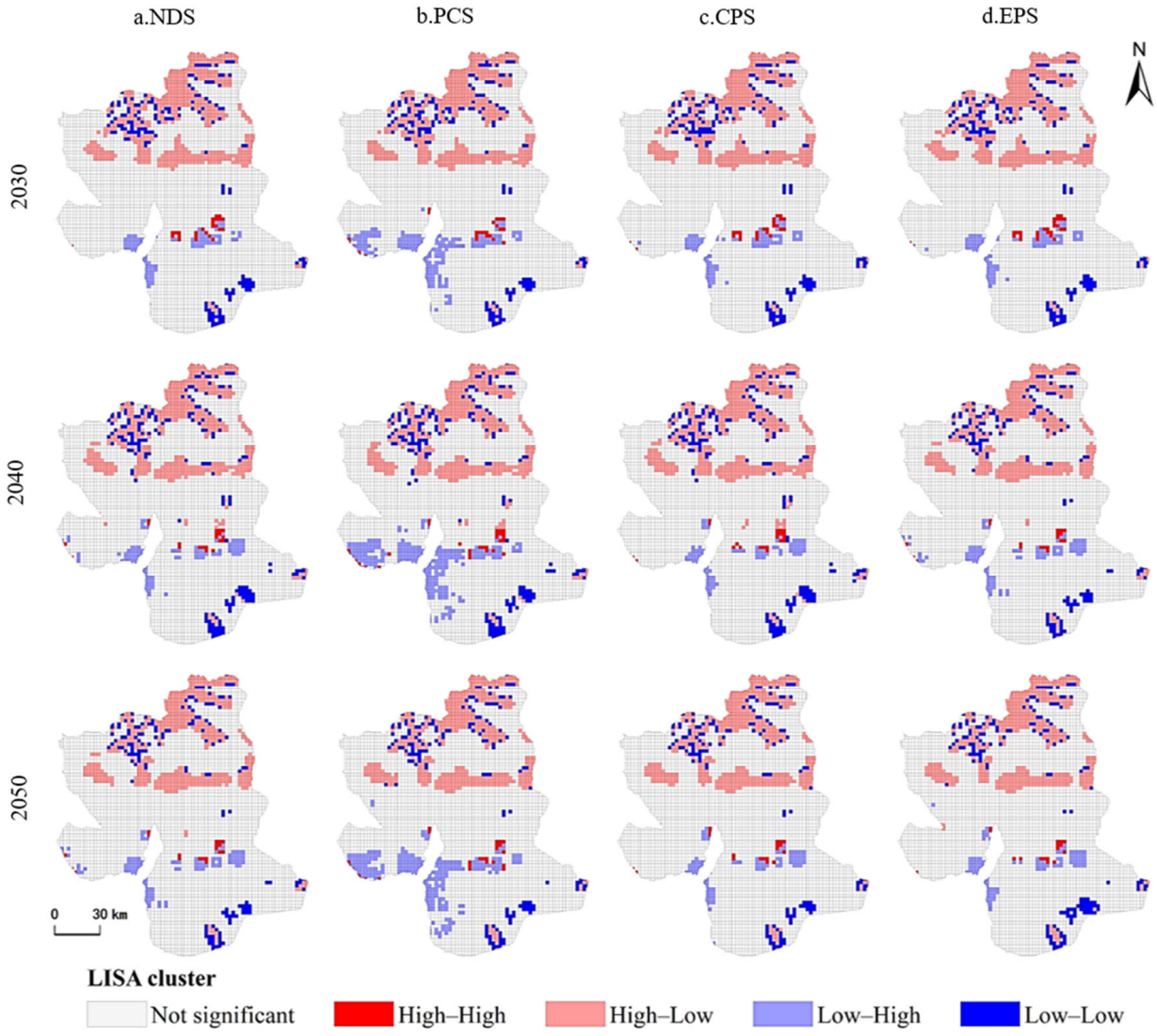

Figure 14. LISA cluster maps of bivariate spatial linkages in Wensu Oasis under natural development (**a**), production and construction (**b**), cultivated land protection (**c**), and ecological protection (**d**) scenarios for the years 2030, 2040, and 2050.

Under NDS, the High–Low clusters in Wensu Oasis show a decreasing trend from 2030 to 2050, with the number of grids declining from 547 in 2030 to 511 in 2050, representing a 7% reduction in area. This indicates that in the absence of policy interventions, economic activities and environmental changes will jointly lead to a reduction in water, thereby reducing ESV. The numbers of High–High and Low–Low clusters also show a slight decreasing trend, with fewer than 15 grid cells each. The number of Low–High clusters fluctuates upward, increasing from 98 grids in 2030 to 103 in 2050. The spatial distribution of High–High, Low–High, and Low–Low clusters remains generally consistent with that of 2020.

Under PCS, the number of Low–High clusters increases significantly from 201 in 2030 to 267 in 2050, representing a 33% increase in area. This suggests that production and construction activities drive large-scale expansion of construction land, thereby increasing regional carbon emissions, and reflects the strong stimulating effect of such activities on carbon emissions. The decreased trend in the number of High–Low clusters becomes more pronounced in 2040 and 2050, indicating a slowdown in the expansion of construction land. Changes in High–High and Low–Low clusters are relatively minor.

Under CPS, the trends for all four types of spatial clusters from 2030 to 2050 are generally similar to those under the natural development scenario, suggesting that changes in cultivated land area have an insignificant impact on regional carbon emissions and ESV.

Under EPS, the High–Low clusters show a decreasing trend from 2030 to 2050, mainly in the northern part of the oasis. This indicates that, in the context of global warming, accelerated glacial melting in northern mountainous areas reduces the amount of water. Meanwhile, the increases in grassland and forest areas are not sufficient to offset the ecological degradation caused by water loss, resulting in a decline in ESV. Additionally, changes in High–High, Low–High, and Low–Low clusters are minimal.

From 2030 to 2050, the coupling coordination levels between land use carbon emission intensity and $\overline{ESV}$ in Wensu Oasis show a downward trend under the four development scenarios. The mean coupling coordination degrees under the natural development, production and construction, cultivated land protection, and ecological protection scenarios decreased by 0.0031, 0.0034, 0.0018, and 0.0007, respectively. The declines are relatively small, and the average coupling coordination degree remains between 0.52 and 0.54, indicating a generally low level of coupling coordination in the future. Therefore, efforts to enhance the coupling and coordinated development between carbon emissions and ecosystem services are necessary.

In terms of spatial distribution (Figure 15), the coupling coordination types of land use carbon emission intensity and $\overline{ESV}$ under the four scenarios in 2030, 2040, and 2050 are largely consistent with the pattern observed over the past 30 years. A clear "high in the north and low in the south" spatial pattern persists, with most areas falling into the stages of moderate disorder and intermediate coordination. Disordered zones tend to expand while coordinated zones tend to shrink, indicating relatively small changes in spatial distribution patterns.

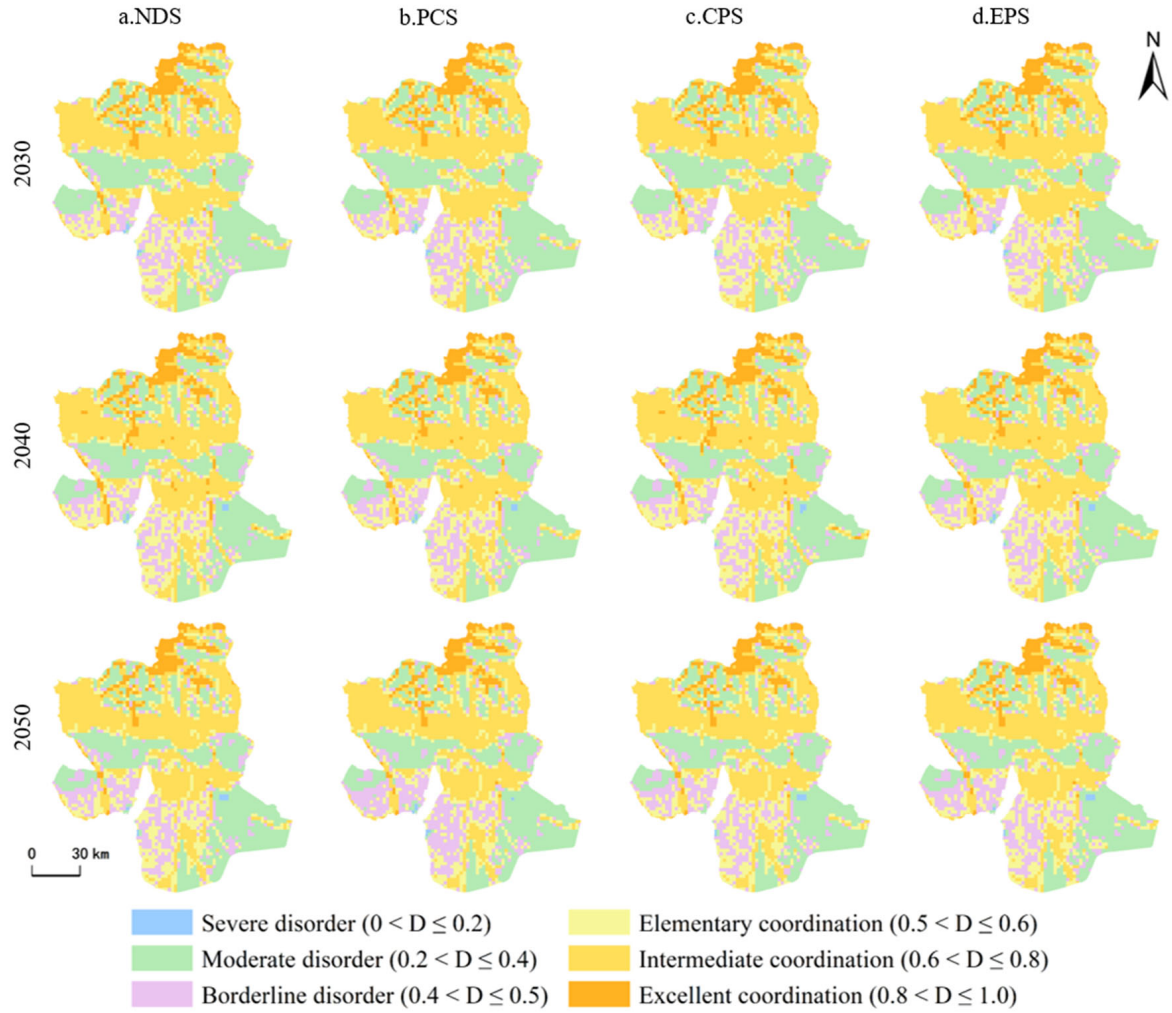

Figure 15. Spatial distribution of coupled coordination types of land use carbon emission intensity and *ESV* intensity in Wensu under natural development (**a**), production and construction (**b**), cultivated land protection (**c**), and ecological protection (**d**) scenarios for the years 2030, 2040, and 2050.

3.6. Sensitivity Analysis of Carbon Emissions and Ecosystem Service Value

To evaluate the robustness of the ESV estimates, a sensitivity analysis was conducted by adjusting the corrected equivalent coefficients of ecosystem services by ±50%. The coefficient of sensitivity (*CS*) values for different land use types in 1990–2020 and under the four future scenarios (2030–2050) are presented in Table 8. The results indicate that water and grassland have the highest sensitivity, with *CS* values consistently greater than 0.3, suggesting that changes in their coefficients have a substantial impact on the total ESV. In contrast, cultivated land, forest, and unused land displayed much lower *CS* values (<0.1), reflecting limited influence on overall ESV outcomes. This pattern implies that assessment of the ESV in the Wensu Oasis is relatively robust; however, the contributions of water and grassland remain a major source of uncertainty.

Furthermore, Table 9 reports the results of the trade-off sensitivity test between ESV and carbon emissions using bivariate Moran's *I* under ±50% adjustments of land use coefficients. Across both historical periods (1990–2020) and scenario-based simulations (2030–2050), Moran's *I* values remained predominantly negative, confirming the persistence of the inverse spatial relationship between carbon emissions and ESV despite large parameter perturbations. Although the absolute values of Moran's *I* varied by year and scenario, the overall pattern consistently indicated a significant trade-off between the two indicators. These results provide strong evidence that the observed carbon–ESV relationship is

robust to parameter uncertainty and that the conclusions drawn in this study are reliable. Therefore, the sensitivity analysis not only validates the robustness of the carbon–ESV trade-off but also highlights that water and grassland are the key sources of uncertainty, which should be given priority in future refinement of ESV coefficient estimations.

Table 8. Sensitivity shares (*CS*) of ecosystem service value by land use class in the Wensu Oasis.

Year	Cultivated Land (CL)	Forest (F)	Grassland (G)	Water (W)	Unused Land (UL)
1990	0.018	0.024	0.322	0.624	0.013
2000	0.022	0.032	0.309	0.625	0.012
2010	0.058	0.034	0.557	0.318	0.034
2020	0.065	0.032	0.466	0.403	0.034
2030NDS	0.070	0.030	0.394	0.473	0.033
2030PCS	0.070	0.030	0.392	0.475	0.034
2030CPS	0.070	0.030	0.394	0.473	0.033
2030EPS	0.070	0.030	0.394	0.473	0.033
2040NDS	0.076	0.029	0.396	0.467	0.031
2040PCS	0.074	0.029	0.398	0.469	0.031
2040CPS	0.078	0.029	0.396	0.466	0.031
2040EPS	0.079	0.036	0.412	0.440	0.033
2050NDS	0.085	0.036	0.427	0.418	0.034
2050PCS	0.081	0.037	0.429	0.419	0.035
2050CPS	0.086	0.036	0.426	0.417	0.034
2050EPS	0.084	0.043	0.425	0.414	0.034

Table 9. Ecosystem service values and carbon emission trade-off sensitivity (bivariate Moran's *I*) to ±50% changes in individual land use coefficients in Wensu Oasis.

Year	CL + 50%	CL − 50%	F + 50%	F − 50%	GL + 50%	GL − 50%	W + 50%	W − 50%	UL + 50%	UL − 50%
1990	−0.117	−0.127	−0.125	−0.118	−0.136	−0.104	−0.074	−0.290	−0.123	−0.121
2000	−0.099	−0.110	−0.106	−0.103	−0.117	−0.090	−0.065	−0.240	−0.106	−0.104
2010	−0.230	−0.335	−0.261	−0.305	−0.317	−0.191	−0.181	−0.480	−0.300	−0.268
2020	−0.013	−0.186	−0.065	−0.137	−0.172	−0.019	−0.067	−0.157	−0.122	−0.081
2030NDS	−0.167	−0.111	−0.136	−0.143	−0.104	−0.168	−0.097	−0.204	−0.136	−0.142
2030PCS	−0.258	−0.241	−0.253	−0.246	−0.246	−0.231	−0.155	−0.491	−0.249	−0.251
2030CPS	−0.169	−0.145	−0.158	−0.156	−0.137	−0.166	−0.103	−0.274	−0.161	−0.154
2030EPS	−0.007	−0.028	−0.013	−0.022	−0.033	−0.003	−0.009	−0.046	−0.019	−0.016
2040NDS	−0.022	−0.038	−0.020	−0.041	−0.050	−0.003	−0.018	−0.062	−0.028	−0.033
2040PCS	−0.145	−0.151	−0.162	−0.133	−0.188	−0.084	−0.068	−0.438	−0.146	−0.151
2040CPS	−0.022	0.009	−0.024	−0.012	−0.048	−0.074	−0.017	−0.066	−0.009	−0.003
2040EPS	−0.107	−0.106	−0.105	−0.108	−0.129	−0.637	−0.550	−0.266	−0.105	−0.109
2050NDS	−0.231	−0.224	−0.385	−0.635	−0.171	−0.272	−0.095	−0.684	−0.228	−0.228
2050PCS	−0.410	−0.487	−0.400	−0.500	−0.105	−0.364	−0.001	−0.252	−0.436	−0.466
2050CPS	−0.143	−0.111	−0.131	−0.122	−0.129	−0.109	−0.665	−0.312	−0.131	−0.123
2050EPS	−0.283	−0.243	−0.271	−0.253	−0.310	−0.166	−0.125	−0.697	−0.259	−0.268

Notes: CL, F, GL, W, and UL represent cultivated land, forest, grassland, water, and unused land, respectively.

4. Discussion

4.1. Impact of Land Use Change on Carbon Emissions and Ecosystem Service Value in Wensu Oasis

The spatiotemporal variations, spatial associations, and clustering patterns of land use carbon emissions and ecosystem service value (ESV) in the Wensu Oasis, a representative oasis in the arid region of northwest China, were analyzed at the grid scale in this study. From 1990 to 2020, the Wensu Oasis experienced substantial land use/cover change (LUCC),

characterized by the continuous expansion of cultivated land, construction land, and unused land, accompanied by the loss of grassland, forest, and water bodies. These changes led to a steady increase in total carbon emissions, particularly in high-intensity emission zones associated with construction land expansion—consistent with the findings of Yang et al. [47], who pointed out that land use changes significantly affect carbon emissions and the carbon sink–source pattern, and that unregulated land development can disrupt carbon cycle balance. The reduction in water bodies and vegetation cover also contributed to the decline in ESV, with the total value decreasing by 46.37% during the study period. Similar patterns have been observed in other oasis regions of arid China, such as the Dunhuang Oasis [48] and Aksu Oasis [49], where agricultural intensification and urban expansion have reduced carbon sequestration capacity and degraded regulating ecosystem services. This consistency suggests that LUCC-driven increases in carbon emissions and decreases in ESV are a common phenomenon in arid oases, reflecting the vulnerability of these systems to intensive land development.

The loss of grassland and forest areas not only diminished their direct carbon storage capacity but also weakened their role in regulating microclimate, soil conservation, and water retention. Likewise, the shrinkage of water bodies directly reduced water-related ESV components and indirectly impacted carbon dynamics by altering soil moisture and vegetation productivity [8,9]. These findings highlight the dual role of LUCC in shaping both the carbon cycle and ecosystem service provision in water-limited environments. At the same time, the LUCC-driven increase in emissions and decline in ESV reflect the practical challenges of meeting China's "dual-carbon" targets under the Action Plan for Carbon Dioxide Peaking before 2030, and underscore the importance of farmland protection redlines in preventing further ecological degradation [50].

Furthermore, external drivers such as climate change and policy interventions also have certain impacts on the future of local land use dynamics [51]. Spatiotemporal climatic change in northwest China is expected to exhibit continuous warming and wetting trends. Climate projections for Xinjiang based on CMIP6 scenarios suggest a gradual warming trend accompanied by modest increases in precipitation through the 2050s [52]. On the policy side, national initiatives—including the National Climate Change Adaptation Strategy 2035, the Action Plan for Carbon Dioxide Peaking before 2030, farmland protection redline regulations, and ecological restoration programs such as the "Grain for Green" project—are exerting increasing influence on land use governance [50]. These measures collectively operationalize China's "dual-carbon" pathway in the land sector, corresponding to SDG 13 (Climate Action) and SDG 15 (Life on Land) [53]. Therefore, at the 2030 horizon, the projected patterns of carbon emissions and ESV are expected to be primarily determined by land use scenarios rather than abrupt climatic shifts or unforeseen policy changes.

4.2. Coupling Characteristics Between Land Use Carbon Emission and Ecosystem Service Value in Wensu Oasis

Spatial correlation analysis for 1990–2020 revealed a significant negative association between carbon emission intensity and ESV, indicating that areas with higher carbon emissions generally exhibit lower ecosystem service value, consistent with findings in the Guanzhong urban agglomeration [24] and the Yellow River Basin [26] in northern China. Nevertheless, the stronger negative correlation in Wensu Oasis reflects its higher dependence on irrigation agriculture and more severe loss of natural vegetation, suggesting that LUCC-induced trade-offs are more pronounced in water-limited environments. In contrast, studies in humid regions such as Guangdong Province in southern China have reported occasional positive correlations between carbon emissions and ESV [25], highlighting that the nature of carbon–ESV interactions is strongly shaped by regional hydrological and ecological conditions. This pattern was most evident in zones experiencing rapid expansion

of construction land, where loss of vegetation cover and water bodies coincided with increased carbon emissions. The *D* between carbon emissions and ESV remained at a low level across the oasis, with a spatial distribution of "high in the north, low in the south." These results suggest that, under current land management practices, carbon reduction and ESV enhancement have not been achieved simultaneously.

The predicted scenarios indicate divergent trajectories. Under the natural development scenario, continued expansion of cultivated and construction land will lead to further increases in carbon emissions and a pronounced decline in ESV, exacerbating the negative correlation and further lowering the *D*. In contrast, an ecological protection scenario—characterized by wetland conservation, grassland restoration, and restrained urban expansion—shows potential for stabilizing or even improving ESV while limiting the growth of carbon emissions. This result resonates with China's National Climate Change Adaptation Strategy 2035 and aligns with international frameworks such as the United Nations Sustainable Development Goals (SDG 13: Climate Action and SDG 15: Life on Land) [53], which emphasize integrated approaches to climate mitigation and terrestrial ecosystem restoration. This scenario results in a weaker negative correlation and, in some grids, a shift toward neutral or slightly positive relationships between the two indicators. These findings underscore the sensitivity of the carbon–ESV relationship to land use policy and management strategies, highlighting that proactive ecological protection measures can substantially improve water–carbon balance and mitigate the trade-offs induced by LUCC.

4.3. Reasonable Strategies for Enhancing Ecosystem Service Value and Reducing Carbon Emissions in Wensu Oasis

Based on the identified mechanisms through which land use change influences carbon emissions and ecosystem service value (ESV), the predicted trends under different development scenarios, and relevant research on the impacts of oasis development in Xinjiang on regional economies and ecological environments [54,55], we proposed the following targeted strategies to promote the sustainable development of the Wensu Oasis agricultural system and to achieve a coordinated water–carbon balance.

(1) Spatially differentiated land use regulation

Land management should be tailored to the spatial heterogeneity of carbon emissions and ESV by implementing zone-specific interventions:

a. Northern glacier-fed water conservation zone (high-ESV–low-emission clusters): Strictly protect glacier and aquatic ecosystems by delineating ecological redlines to prevent encroachment from cultivated and construction land. Priority should be given to maintaining their core carbon sequestration function (contributing 63.8% of total carbon uptake) and hydrological regulation capacity (accounting for 71% of the water regulation value). Measures should include establishing a seasonal ecological water replenishment mechanism, targeted restoration of degraded wetlands, and enhancement of soil carbon sequestration potential [56].
b. Southern intensive agricultural production zone (low-ESV–high-emission clusters): promote water-saving and emission-reduction technologies [57], such as adopting mulched drip irrigation in cotton fields to reduce agricultural water consumption; optimize cropping patterns by converting marginal farmland into agroforestry systems (e.g., walnut–alfalfa intercropping) to improve both economic returns and carbon sequestration; restrict the uncontrolled expansion of construction land; and reduce irrigation-related energy emissions [58].
c. Central ecological transition zone: Implement degraded grassland restoration projects, plant drought-tolerant shrubs and grasses (e.g., Tamarix spp.) to improve soil and water conservation, and establish riparian shelterbelt buffer zones to mitigate the neg-

ative impacts of agricultural non-point source pollution on the carbon sequestration capacity of water bodies.

(2) Scenario-oriented land use optimization

a. Ecological protection scenario (EPS) as a priority: converting cropland to wetlands can substantially restore aquatic ecosystem functions and promote synergistic gains in water and carbon regulation. Model simulations indicate that this strategy could enhance regional carbon sequestration by 27.6% and achieve a balance between ecological benefits and agricultural production.

b. Refinement of the cultivated land protection scenario (CPS): concentrate newly allocated cropland quotas in high-efficiency, water-saving farmland and equip these areas with advanced irrigation infrastructure. This approach can avoid the unsustainable "water-for-grain" development pathway. Furthermore, strictly limit cropland expansion into water bodies to safeguard the ecological water-use baseline.

4.4. Limitations

The estimation of ESV relied on coefficient-based methods, which inevitably simplify ecological heterogeneity. Secondly, carbon emissions were calculated using the emission coefficient approach, which does not account for dynamic carbon fluxes such as soil respiration or vegetation growth responses. Moreover, the PLUS model simulations were based on historical LUCC drivers and scenario assumptions, without explicitly incorporating uncertainties associated with future climate change or socioeconomic development. Future research could benefit from integrating higher-resolution ecological datasets, process-based carbon models, and multi-scenario socio-ecological drivers to reduce uncertainties and enhance the robustness of the findings.

5. Conclusions

(1) The Wensu Oasis underwent significant land use/cover change from 1990 to 2020, characterized by the continuous expansion of cultivated land, construction land, and unused land, accompanied by reductions in grassland, forest, and water bodies. The most pronounced changes occurred between 2000 and 2010.

(2) Carbon emission intensity has increased steadily, with high-value zones expanding in close association with the growth of construction land over the past three decades; conversely, the total ESV has declined by 46.37%, with water and grassland making substantial contributions to the loss. Spatially, carbon emission intensity and ESV exhibit a significant negative correlation, and the coupling coordination degree remains low, following a "high in the north, low in the south" pattern.

(3) Under scenarios of natural development, production and construction, cultivated land protection, and ecological protection for 2030, 2040, and 2050, the negative correlation between carbon emissions and ESV is likely to persist. Although the coupling coordination degree remains between 0.52 and 0.54, a slight downward trend is observed, indicating that without targeted interventions, coordinated improvement of carbon mitigation and ESV enhancement will be difficult to achieve.

(4) Based on the spatial clustering of carbon emissions and ESV, and in light of predicted scenario outcomes, we recommend implementing spatially differentiated land use regulation and prioritizing the ecological protection scenario to restore aquatic ecosystems, improve carbon sequestration capacity, and promote synergistic water–carbon benefits.

(5) Ecological protection measures, including wetland conservation, grassland restoration, and water-saving agricultural technologies, should be prioritized in the future to mitigate carbon emissions and enhance ecosystem services. At the same time, scenario-

oriented land use optimization should be incorporated into regional planning to reconcile agricultural productivity with ecological sustainability, thereby ensuring the long-term resilience of oasis socio-ecological systems.

Author Contributions: Conceptualization, Y.Z., S.N. and J.S.; methodology, Y.Z., H.R., N.L. and T.H.; software, Y.Z.; validation, Y.Z.; formal analysis, Y.Z. and H.R.; investigation, Y.Z.; resources, Y.Z.; data curation, Y.Z., N.L. and T.H.; writing—original draft preparation, Y.Z., S.N. and A.Y.; writing—review and editing, S.N., A.Y., P.J. and J.S.; visualization, Y.Z., N.L. and T.H.; supervision, S.N. and A.Y.; project administration, S.N., A.Y., J.S. and P.J.; funding acquisition, S.N. and P.J. All authors have read and agreed to the published version of the manuscript.

Funding: This research was funded by the Key Research and Development Program of the Xinjiang Uygur Autonomous Region (2023A02002-2 and 2024B03023-3), the National Natural Science Foundation of China (32160527), and the Natural Science Foundation of Xinjiang Uygur Autonomous Region (2025D01D17).

Data Availability Statement: The data supporting the findings of this study are available from the first author upon reasonable request.

Acknowledgments: The authors are grateful to the anonymous reviewers and the editor for their helpful and constructive comments and suggestions, which have improved the manuscript.

Conflicts of Interest: The authors declare no conflicts of interest.

References

1. Tang, Y.; Xia, N.; Xiao, Y.; Xu, Z.; Ma, Y. Assessment of crop water resource utilization in arid and semi-arid regions based on the water footprint theory. *Agronomy* **2025**, *15*, 1529. [CrossRef]
2. Liu, X.; Wang, Y.; Xin, L. China's oases have expanded by nearly 40% over the past 20 years. *Land Degrad. Dev.* **2022**, *33*, 3817–3828. [CrossRef]
3. Zhang, Y.; Wang, L.; Zhao, W.; Zhao, X.; Wang, C.; Kang, W.; Halmy, M.W.A. Rapid global artificial oasis expansion and consequences in arid regions over the last 20 years. *Sci. Bull.* **2025**, *70*, 1949–1952. [CrossRef]
4. Sannigrahi, S.; Pilla, F.; Zhang, Q.; Chakraborti, S.; Wang, Y.; Basu, B.; Basu, A.S.; Joshi, P.K.; Keesstra, S.; Roy, P.S.; et al. Examining the effects of green revolution led agricultural expansion on net ecosystem service values in India using multiple valuation approaches. *J. Environ. Manag.* **2021**, *277*, 111381. [CrossRef]
5. Zhao, N.; Du, L.; Tian, S.; Zhang, B.; Zheng, X.; Li, Y. Cropland expansion masks ecological degradation: The unsustainable greening of China's drylands. *Agronomy* **2025**, *15*, 1162. [CrossRef]
6. Tang, J.; Gong, L.; Ma, X.; Zhu, H.; Ding, Z.; Luo, Y.; Zhang, H. The oasisization process promotes the transformation of soil organic carbon into soil inorganic carbon. *Land* **2024**, *13*, 336. [CrossRef]
7. Xu, E.; Zhang, H.; Xu, Y. Effect of large-scale cultivated land expansion on the balance of soil carbon and nitrogen in the Tarim Basin. *Agronomy* **2019**, *9*, 86. [CrossRef]
8. Li, W.; Xiang, M.; Duan, L.; Liu, Y.; Yang, X.; Mei, H.; Wei, Y.; Zhang, J.; Deng, L. Simulation of land utilization change and ecosystem service value evolution in Tibetan area of Sichuan Province. *Alex. Eng. J.* **2023**, *70*, 13–23. [CrossRef]
9. Guan, Y.; Jin, S.; Zhang, Z.; Chen, S.; Chen, Y.; Liu, S.; Fan, M.; Ding, Y.; Yuan, X. A comprehensive review of climate warming and carbon dynamics in wetland ecosystems. *Discov. Sustain.* **2025**, *6*, 672. [CrossRef]
10. Liu, J.; Pei, X.; Zhu, W.; Jiao, J. Multi-scenario simulation of carbon budget balance in arid and semi-arid regions. *J. Environ. Manag.* **2023**, *346*, 119016. [CrossRef]
11. Feng, X.; Li, Y.; Yu, E.; Yang, J.; Wang, S.; Ma, J. Spatiotemporal pattern and coordinating development characteristics of carbon emission performance and land use intensity in the Yangtze River Delta Urban Agglomeration. *Trans. Chin. Soc. Agric. Eng.* **2023**, *39*, 208–218. [CrossRef]
12. Ke, N.; Lu, X.; Zhang, X.; Kuang, B.; Zhang, Y. Urban land use carbon emission intensity in China under the "double carbon" targets: Spatiotemporal patterns and evolution trend. *Environ. Sci. Pollut. Res.* **2022**, *30*, 18213–18226. [CrossRef]
13. Liu, X.J.; Jin, X.B.; Luo, X.L.; Zhou, Y.K. Multi-scale variations and impact factors of carbon emission intensity in China. *Sci. Total Environ.* **2023**, *857*, 159403. [CrossRef]
14. Han, Y.; Ge, X. Spatial–temporal characteristics and influencing factors on carbon emissions from land use in Suzhou, the world's largest industrial city in China. *Sustainability* **2023**, *15*, 13306. [CrossRef]

15. Liu, C.; Hu, S.; Wu, S.; Song, J.; Li, H. County-level land use carbon emissions in China: Spatiotemporal patterns and impact factors. *Sustain. Cities Soc.* **2024**, *105*, 105304. [CrossRef]
16. Rong, T.; Zhang, P.; Zhu, H.; Jiang, L.; Li, Y.; Liu, Z. Spatial correlation evolution and prediction scenario of land use carbon emissions in China. *Ecol. Inform.* **2022**, *71*, 101802. [CrossRef]
17. Gui, D.; He, H.; Liu, C.; Han, S. Spatio-temporal dynamic evolution of carbon emissions from land use change in Guangdong Province, China, 2000–2020. *Ecol. Indic.* **2023**, *156*, 111131. [CrossRef]
18. Ge, K.; Wang, Y.; Liu, X.; Hu, L.; Ke, S.; Jiang, X.; Zhang, W. Spatial effects and influence mechanisms of urban land use green transition on urban carbon emissions. *Ecol. Indic.* **2025**, *172*, 113261. [CrossRef]
19. Pu, L.; Lu, C.; Yang, X.; Chen, X. Spatio-temporal variation of the ecosystem service value in Qilian mountain national park (Gansu area) based on land use. *Land* **2023**, *12*, 201. [CrossRef]
20. Chi, Y.; He, C. Impact of land use change on the spatial and temporal evolution of ecosystem service values in south China Karst Areas. *Forests* **2023**, *14*, 893. [CrossRef]
21. Yang, Y.; Qin, T.; Yan, D.; Liu, S.; Feng, J.; Wang, Q.; Liu, H.; Gao, H. Analysis of the evolution of ecosystem service value and its driving factors in the Yellow River Source Area, China. *Ecol. Indic.* **2024**, *158*, 111344. [CrossRef]
22. Zhou, X.; Ji, G.; Wang, F.; Ji, X. Identification and simulation of ecological zoning in the Yangtze River Delta (YRD) urban agglomeration based on ecological service value (ESV)–landscape ecological risk (LER). *J. Clean. Prod.* **2025**, *516*, 145778. [CrossRef]
23. Zhang, M.; Chen, E.; Zhang, C.; Liu, C.; Li, J. Multi-Scenario simulation of land use change and ecosystem service value based on the Markov–FLUS Model in Ezhou City, China. *Sustainability* **2024**, *16*, 6237. [CrossRef]
24. Zhang, R.; Yu, K.; Luo, P. Spatio-temporal relationship between land use carbon emissions and ecosystem service value in Guanzhong, China. *Land* **2024**, *13*, 118. [CrossRef]
25. Lang, Y.; Chao, H.; Xiao, J. The relationship between carbon emissions and ecosystem services in Guangdong Province, China: The perspective of ecological function zones. *Land* **2024**, *13*, 2227. [CrossRef]
26. Chen, H.; Jiang, L.; Wang, Z. Spatial temporal coupling and influencing factors of land-use carbon emissions and ecosystem service value in the Yellow River Basin. *Environ. Sci.* **2025**, *46*, 3536–3545. [CrossRef]
27. Dhawi, F.; Aleidan, M.M. Oasis agriculture revitalization and carbon sequestration for climate-resilient communities. *Front. Agron.* **2024**, *6*, 1386671. [CrossRef]
28. Kalfas, D.; Kalogiannidis, S.; Papaevangelou, O.; Chatzitheodoridis, F. Assessing the connection between land use planning, water resources, and global climate change. *Water* **2024**, *16*, 333. [CrossRef]
29. Fu, S.; Xu, B.; Peng, Y.; Wang, H.; Li, X. Analysis of spatiotemporal coupling relationship between carbon emission and ecosystem service value in Poyang Lake Basin based on land use. *Res. Soil Water Conserv.* **2025**, *32*, 321–331+342. [CrossRef]
30. Tan, Z.; Guan, Q.; Lin, J.; Yang, L.; Luo, H.; Ma, Y.; Tian, J.; Wang, Q.; Wang, N. The response and simulation of ecosystem services value to land use/land cover in an oasis, Northwest China. *Ecol. Indic.* **2020**, *118*, 106711. [CrossRef]
31. Zhang, T.; Xiao, P.; Yang, Z.; Guo, J. Status identification and restoration zoning of ecological space in Maowusu Sandy Land based on temporal and spatial characteristics of land use. *Agronomy* **2025**, *15*, 1445. [CrossRef]
32. He, J.; Zhang, P. Evaluation of carbon emissions associated with land use and cover change in Zhengzhou City of China. *Reg. Sustain.* **2022**, *3*, 1–11. [CrossRef]
33. Zhang, J.; Zhang, C.; Dong, H.; Zhang, L.; He, S. Spatial–temporal change analysis and Multi-Scenario simulation prediction of land-use carbon emissions in the Wuhan Urban Agglomeration, China. *Sustainability* **2023**, *15*, 11021. [CrossRef]
34. Han, F.; Gao, F.; He, B.; Cao, Y.; Yao, X. Exploring the spatial and temporal trajectories of land use carbon emissions and influencing factors in the Aksu River Basin from 1990 to 2020. *Environ. Sci.* **2024**, *45*, 3297–3307. [CrossRef]
35. Fang, J.; Guo, Z.; Piao, S.; Chen, A. Estimation of terrestrial vegetation carbon sequestration in China from 1981 to 2000. *Sci. China Ser. D Earth Sci.* **2007**, *37*, 804–812. [CrossRef]
36. Xie, G.; Zhang, C.; Zhang, L.; Chen, W.; Li, S. Improvement of the evaluation method for ecosystem service value based on per unit area. *J. Nat. Resour.* **2015**, *30*, 1243–1254. [CrossRef]
37. Cheng, W.; Shen, B.; Xin, X.; Gu, Q.; Guo, T. Spatiotemporal Variations of Grassland Ecosystem Service Value and Its Influencing Factors in Inner Mongolia, China. *Agronomy* **2022**, *12*, 2090. [CrossRef]
38. Li, X.; Wu, C. Sensitivity assessment and simulation of ecosystem services in response to land use change in arid regions: Empirical evidence from Xinjiang, China. *Ecol. Indic.* **2025**, *171*, 113150. [CrossRef]
39. Mamat, A.; Wang, J.; Aimaiti, M.; Saydi, M. Evolution and driving forces of ecological service value in response to land ese change in Tarim Basin, Northwest China. *Remote Sens.* **2024**, *16*, 2311. [CrossRef]
40. Ma, J.; Wen, J.; Du, S.; Yan, C.; Pan, C. Spatiotemporal evolution of carbon storage and driving factors in major sugarcane-producing regions of Guangxi, China. *Agronomy* **2025**, *15*, 1817. [CrossRef]
41. Wei, S.; Hou, J.; Zhang, Y.; Tai, Y.; Huang, X.; Guo, X. Analysis of the trade-off/synergy effect and driving factors of ecosystem services in Hulunbuir City, China. *Agronomy* **2025**, *15*, 1883. [CrossRef]

42. Zhao, S.; Yu, Z.; Liu, W. Revealing the spatio-temporal coupling coordination characteristics and influencing factors of carbon emissions from urban use and ecosystem service values in China at the municipal scale. *Front. Ecol. Evol.* **2025**, *13*, 1539909. [CrossRef]
43. Rong, T.; Zhang, P.; Li, G.; Wang, Q.; Zheng, H.; Chang, Y.; Zhang, Y. Spatial correlation evolution and prediction scenario of land use carbon emissions in the Yellow River Basin. *Ecol. Indic.* **2023**, *154*, 110701. [CrossRef]
44. Wu, Q.; Wang, L.; Wang, T.; Ruan, Z.; Du, P. Spatial–temporal evolution analysis of multi-scenario land use and carbon storage based on PLUS-InVEST model: A case study in Dalian, China. *Ecol. Indic.* **2024**, *166*, 112448. [CrossRef]
45. Wu, X.; Shen, C.; Shi, L.; Wan, Y.; Ding, J.; Wen, Q. Spatio-temporal evolution characteristics and simulation prediction of carbon storage: A case study in Sanjiangyuan Area, China. *Ecol. Inform.* **2024**, *80*, 102485. [CrossRef]
46. Peng, W.F.; Zhou, J.M.; Fan, S.Y.; Yang, C.J. Effects of the land use change on ecosystem service value in Chengdu, Western China from 1978 to 2010. *J. Indian Soc. Remote Sens.* **2015**, *44*, 197–206. [CrossRef]
47. Yang, S.; Zheng, X. Spatio-temporal relationship between carbon emission and ecosystem service value under land use change: A case study of the Guanzhong Plain Urban Agglomeration, China. *Front. Environ. Sci.* **2023**, *11*, 1241781. [CrossRef]
48. Yi, F.; Yang, Q.; Wang, Z.; Li, Y.; Cheng, L.; Yao, B.; Lu, Q. Changes in land use and ecosystem service values of Dunhuang Oasis from 1990 to 2030. *Remote Sens.* **2023**, *15*, 564. [CrossRef]
49. Yang, J.; Gao, F.; Xu, H.; Liu, K.; Han, F. Spatial and temporal evolution of ecosystem service value and its driving factors in the Aksu River Basin. *Environ. Sci.* **2025**, *46*, 2385–2397. [CrossRef]
50. Chen, Y.; Zhao, X.; Wu, S.; Tong, Z. Developing ecological protection redline policy for land use pattern optimization in the typical black soil region of Northeastern China. *Front. Environ. Sci.* **2024**, *12*, 1422077. [CrossRef]
51. Tölgyesi, C.; Csikós, N.; Temperton, V.M.; Buisson, E.; Silveira, F.A.O.; Lehmann, C.E.R.; Török, P.; Bátori, Z.; Bede-Fazekas, Á. Limited carbon sequestration potential from global ecosystem restoration. *Nat. Geosci.* **2025**, *18*, 761–768. [CrossRef]
52. Song, X.; Xu, M.; Kang, S.; Wang, R.; Wu, H. Evaluation and projection of changes in temperature and precipitation over Northwest China based on CMIP6 models. *Int. J. Climatol.* **2024**, *44*, 5039–5056. [CrossRef]
53. Fu, B.; Liu, Y.; Meadows, M.E. Ecological restoration for sustainable development in China. *Natl. Sci. Rev.* **2023**, *10*, 60–71. [CrossRef] [PubMed]
54. Zhou, H.; Wu, B.; Wang, Y.; Li, Y. Ecological achievement of Xinjiang production and construction corps and its problems and countermeasures. *Bull. Chin. Acad. Sci.* **2017**, *32*, 55–63. [CrossRef]
55. Fan, Z.; Wu, S.; Wu, Y.; Zhang, P.; Zhao, X.; Zhang, J. The land reclamation in Xinjiang since the founding of new China. *J. Nat. Resour.* **2013**, *28*, 713–720. [CrossRef]
56. Chen, Y.; Zhang, X.; Fang, G.; Li, Z.; Wang, F.; Qin, J.; Sun, F. Potential risks and challenges of climate change in the arid region of northwestern China. *Reg. Sustain.* **2020**, *1*, 20–30. [CrossRef]
57. Abuduaini, A.; Ren, Q.; Wang, Y.; Yu, J.; Long, A.; Zhang, J. Analysis on the matching characteristics and stability of oasis water and land resources in the Tarim River Basin. *J. China Inst. Water Resour. Hydropower Res.* **2022**, *20*, 71–78. [CrossRef]
58. Sequeira, E.; Leão de Sousa, P.; Correia, A.M.; Rolim, J. The current status of irrigated agriculture in cape verde and its link to water scarcity. *Agronomy* **2025**, *15*, 1625. [CrossRef]